SYNTHESIS OF DIOXIN & TETRA ARYL PYRAZINE DERIVATIVES AND THEIR APPLICATIONS

A THESIS SUBMITTED TO
THE GRADUATE SCHOOL OF NATURAL AND APPLIED SCIENCES
OF
MIDDLE EAST TECHNICAL UNIVERSITY

BY

BURCU OKYAR

IN PARTIAL FULFILLMENT OF THE REQUIREMENTS
FOR
THE DEGREE OF MASTER OF SCIENCE
IN
CHEMISTRY

JANUARY 2019

Approval of the thesis:

SYNTHESIS OF DIOXIN & TETRA ARYL PYRAZINE DERIVATIVES AND THEIR APPLICATIONS

submitted by **BURCU OKYAR** in partial fulfillment of the requirements for the degree of **Master of Science in Chemistry Department, Middle East Technical University** by,

Prof. Dr. Halil Kalıpçılar
Dean, Graduate School of **Natural and Applied Sciences**

Prof. Dr. Cihangir Tanyeli
Head of Department, **Chemistry**

Assist. Prof. Dr. Salih Özçubukçu
Supervisor, **Chemistry, METU**

Assoc. Prof. Dr. Emrullah Görkem Günbaş
Co-Supervisor, **Chemistry, METU**

Examining Committee Members:

Prof. Dr. Cihangir Tanyeli
Chemistry, METU

Assist. Prof. Dr. Salih Özçubukçu
Chemistry, METU

Prof. Dr. Ali Çırpan
Chemistry, METU

Assoc. Prof. Dr. Emrullah Görkem Günbaş
Chemistry, METU

Assist. Prof. Dr. Safacan Kölemen
Chemistry, Koç University

Date: 11.01.2019

I hereby declare that all information in this document has been obtained and presented in accordance with academic rules and ethical conduct. I also declare that, as required by these rules and conduct, I have fully cited and referenced all material and results that are not original to this work.

Name, Surname: BURCU OKYAR

Signature:

ABSTRACT

SYNTHESIS OF DIOXIN & TETRA ARYL PYRAZINE DERIVATIVES AND THEIR APPLICATIONS

OKYAR, BURCU
Master of Science, Chemistry
Supervisor: Assist. Prof. Dr. Salih Özçubukçu
Co-Supervisor: Assoc. Prof. Dr. Emrullah Görkem Günbaş

January 2019, 63 pages

Aggregation induced emission (AIE) luminogens have attracted great attention in various disciplines of science in last decades. The photophysical properties and structural design of this type of luminogens make it possible to have large variety of applications in fluorescence sensors, cell imaging, microstructures aggregate and electroluminescence devices etc. All these studies promote researchers to find alternative AIE luminogens and also different application areas of AIE luminogen systems.

2,3,5,6-tetraphenylpyrazine (TPP) has an interesting structure with its propeller shape and with its planar core. In this conformation, the planarity of each ring is preserved, and the conjugation between the rings is preserved to some extent. Inspired from TPP, in this thesis, 2,3,5,6-tetraphenyl-1,4-dioxine (TPD) was synthesized and AIE property was investigated.

In the second part of the thesis, 2,5-bis(4-bromophenyl)-3,6-diphenylpyrazine (2Br-TPP) was synthesized and will be used in electrochromic devices. It will be polymerized with 3,3-bis((undecyloxy)methyl)-3,4-dihydro-2H-thieno[3,4b][1,4]dioxepine and used in electrochromic device.

In the third part of the thesis, 2,3,5,6-tetrakis(4-bromophenyl) pyrazine (4Br-TPP) was synthesized and coupled with bis(4-methoxyphenyl) amine and the product will be used in perovskite solar cell application as a hole transport material (HTM).

Keywords: Aggregation Induced Emission, Perovskite Solar Cell, Hole Transport Material, Electrochromic Device.

ÖZ

DİOKZİN VE TETRA ARİL PİRAZİN TÜREVLERİNİN SENTEZİ VE UYGULAMA ALANLARI

OKYAR, BURCU
Yüksek Lisans, Kimya
Tez Danışmanı: Dr. Öğr. Üyesi Salih Özçubukçu
Ortak Tez Danışmanı: Doç. Dr. Emrullah Görkem Günbaş

Ocak 2019, 63 sayfa

Kümeleşme ile tetiklenmiş emisyon özelliğine sahip luminojenler son yıllarda, bilimin pek çok alanında büyük ilgi görmüştür. Fotofiziksel özellikleri ve yapısal düzenleri, floresan sensör, hücre görüntüleme, mikro yapıdaki kümeleşmeler, elektroluminesans cihazlar ve daha pek çok uygulama alanında kullanılmasına olanak sağlar. Tüm bu çalışmalar, araştırmacıları kümeleşme ile tetiklenmiş emisyon özelliğine sahip yeni moleküllerin sentezine ve farklı alanlardaki uygulamalarına yönlendirmiştir.

2,3,5,6-tetrafenilpirazin (TPP) molekülü pervane yapısıyla ve düzlemsel merkez halkasıyla sıradışı bir moleküldür. Bu konformasyonda, her bir halkanın düzlemsel yapısı korunurken aynı zamanda halkalar arası konjugasyon da bir noktaya kadar devam etmektedir. Bu molekülün yapısından esinlenerek, 2,3,5,6-tetrafenildiokzin (TPD), sentezlenip kümeleşme ile tetiklenmiş emisyon özelliğine bakılmıştır.

Çalışmanın ikinci kısmında, 2,5-bis(4-bromofenil)-3,6-difenilpirazin (2Br- TPP), elektrokromik cihaz içerisinde kullanılmak üzere sentezlenmiştir. Bu molekül, 3,3-bis((undesiloksi)metil)-3,4-dihidro-2H-tieno[3,4][1,4]diokzepin ile polimerleştirilip elektrokromik cihazlarda kullanılacaktır.

Çalışmanın üçüncü kısmında, perovskit güneş pillerinde delik geçirgen tabaka olarak kullanılmak üzere 2,3,5,6-tetrakis(4-bromofenil) pirazin (4Br- TPP), bis(4-metoksifenil)amin ile bağlanmıştır.

Anahtar Kelimeler: Kümeleşme ile Tetiklenmiş Emisyon, Perovskit Güneş Pili, Elektrokromik Cihaz, Delik Geçirgen Tabaka

To my beloved family

ACKNOWLEDGMENTS

I would like to express my honest gratitude to my supervisor Assist. Prof. Dr. Salih Özçubukçu and my co-advisor Assoc. Prof. Dr. Emrullah Görkem Günbaş for their special guidance and infinite encouragement. It would have been impossible for me to conclude this work without their endless patience and priceless advices. It has been a great honor for me to be a part of Özçubukçu Research Group as a graduate student. It was also a great pleasure to work with Günbaş Research Group in this joint project.

I also would like to thank every single member of Özçubukçu Research group, Dr. Melek Parlak, Dr. Aytül Saylam, Güzide Aykent, Tuğçe Yılmaz, Muzaffer Gökçe, Volkan Dolgun, M. Seçkin Kesici and Medine Soydan for their precious friendship, helps and encouragements.

I also would like to thank Figen Varlıoğlu and Dr. Hava Kaya from Günbaş Research Group for the investigation of Electrochromic Device and Perovskite Solar Cell applications.

I would like to thank Assist. Prof. Dr. Ferdi Karadaş and Dr. Gülsüm Gündoğdu for single crystal X-ray diffractometer analysis.

I would like to thank Prof. Dr. Ahmet Önal and his group members for instrumental usage (Fluorescence Spectrometry).

I wish to thank NMR specialist Betül Eymur for NMR analysis in our department.

I wish to express my gratitude to the academic stuff of Department of Chemistry at METU for their supports and guidance throughout my whole undergraduate and graduate years.

A special thanks to my friends, Ceren Sönmez Özer and Gaye Elbir for their priceless friendships.

Finally, I would thank my family for their endless love and support.

TABLE OF CONTENTS

CHAPTERS

LIST OF TABLES

LIST OF FIGURES

LIST OF SCHEMES

LIST OF ABBREVIATIONS

AIE	Aggregation Induced Emission
ACQ	Aggregation Caused Quenching
TPD	Tetraphenyl dioxin
TPP	Tetraphenyl pyrazine
2Br-TPP	2,5-bis(4-bromophenyl)-3,6-diphenylpyrazine
4Br-TPP	2,3,5,6-tetrakis(4-bromophenyl) pyrazine
EtOAc	Ethyl acetate
THF	Tetrahydrofuran
***t*-BuOH**	*tert*-Butanol
***p*-TsOH**	*para*-Toluene sulfonic acid
NH_4OAc	Ammonium acetate
HRMS	High-resolution Mass Spectrometry
HTM	Hole Transport Material
ETM	Electron Transfer Material
OFET	Organic Field-effect Transistor
OTFT	Organic Thin-film Transistor
OLED	Organic Light Emitting Diode
TLC	Thin Layer Chromatography
TMS	Tetramethylsilane
TTIP	Titanium(IV) isopropoxide

CHAPTER 1

INTRODUCTION

1.1. Luminescence

Luminescence is an attractive phenomenon in fields of chemistry, biology, medicine and physics. In the general mechanism of luminescence, the electrons are excited by UV/visible light and energy is absorbed by the electrons, then these particles spontaneously turn to their ground state, during this process they emit light by some external or internal process (Figure 1.1) [1].

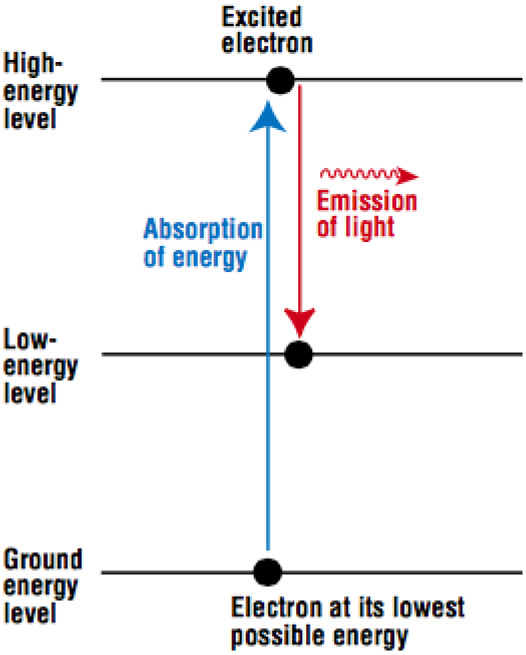

Figure 1.1. Basic Jablonski Diagram

Organic luminescent systems and molecules have attracted considerable attention of many scientists due to their intriguing structural diversity and their potential uses in various applications in optoelectronic and biological fields [2-8]. Light emitting diodes, active semiconductors [9,10], semiconductor microlasers [11], OLEDs (organic light emitting diodes) and OTFTs (organic thin-film transistors) [12] are well-known examples of optoelectronics that utilize organic luminescent systems. Additionally, their prominent use in biological fields are tumor imaging by near-infrared fluorescent Pdots [13], highly sensitive bioimaging fluorescence probe for nitric oxide [8] and AIE based light-up bioprobes [14].

1.1.1. Luminescence Types

Luminescence can be basically categorized into five parts according to source and nature of their excitation (Figure 1.2) [15]. These are photoluminescence, electroluminescence, chemiluminescence, radioluminescence and thermoluminescence. Photoluminescence is triggered by the absorption of UV radiation, then spontaneous emission of light in UV-Vis or near IR region [15]. Photoluminescence is further divided into two parts according to their emission time, fluorescence and phosphorescence. Fluorescence is the first type of photoluminescence; the molecule only emits light during the exposure of radiation of various types- gamma rays, X-rays, UV light, visible light and other types of particles [16]. Phosphorescence is another type of photoluminescence; whose principle is same as fluorescence only differs from emission time. In other words, a molecule continues to give an emission after the excitation radiation is cut off [17]. Electroluminescence is the second category of luminescence, which is caused by the electron bombardment through the material according to the recent terminology [18]. As the electrons strike to solid or liquid, emission of light is occurred. Electroluminescence has also a subtitle which is named as triboluminescence. Triboluminescence is related to the crystals [19]. The surface of the crystals is bombarded with electrons and during this process they emit light.

Triboluminescence is also named as piezoluminescence due to crushing or rubbing of crystals can cause light emission [15]. Triboluminescence is categorized into two parts which are sonoluminescence and crytalloluminescence. Sonoluminescence is, as the sound waves are going through the liquid they tend to form gas cavities in that media. These gas cavities are filled by the electrical discharges and during this process emission of light takes place [20]. As a second type of triboluminescence is crystalloluminescence. The material gives an emission during the formation of crystals in solution [21]. The third category of luminescence is chemiluminescence. This type of emission is caused by the chemical reaction [22]. The emission takes place either in gas or in solution phase. The well-known chemiluminescent is elemental white phosphorus. This material is oxidized in moist air, which causes a green glow [15]. Chemiluminescence has a sub-category called bioluminescence. Bioluminescence is defined as an emission of light by chemiluminesce in living organisms [23]. This type of luminescence is widely seen in marine organisms. Radioluminescence is the fourth category of the luminescence, which is also named as scintillation [15]. In this process, emission of light occurs when the substances are excited with inducers different than light. These inducers can be α-, β, γ-rays, X-rays [24]. The final category of luminescence is thermoluminescence. Firstly, to define a thermoluminescence property of a material, it must be an insulator or a semiconductor [25]. Thermoluminescence is the emission of light, when the substance is heated relatively lower temperatures. Relatively low temperatures are dependent on the incandescence points. In other word, the heating must be way below the incandescence temperatures [15].

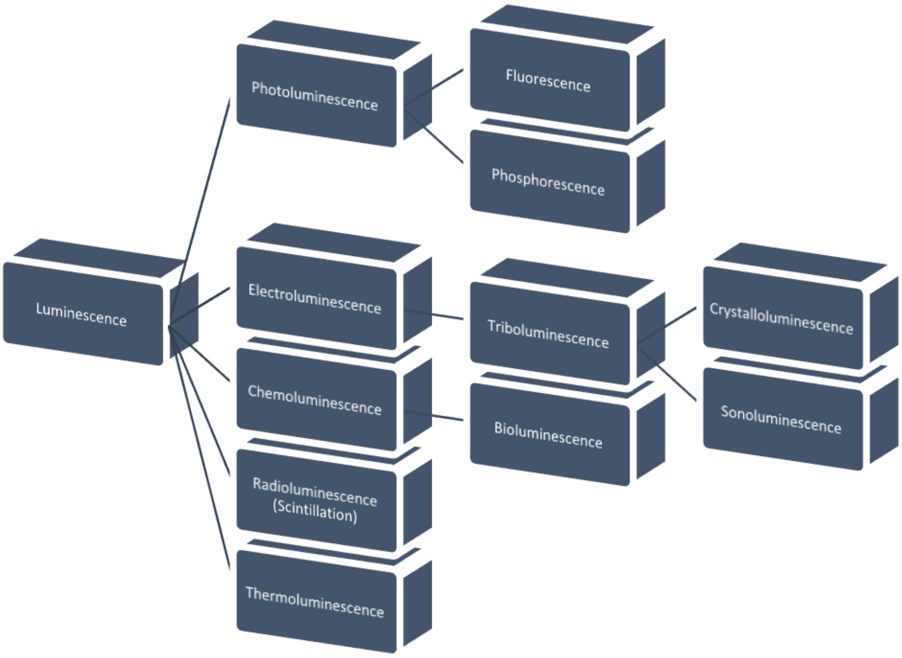

Figure 1.2. Classification of Luminescence.

1.1.2. Fluorophores

Fluorescence is an intriguing issue in many disciplines of science as mentioned above. Generally, a molecule which gives a fluorescence is called fluorophores. Fluorophores can be either organic or inorganic. Organic fluorophores have remarkable significance due to their wide application areas. A small modification in their structure can cause a significant change in their fluorescence properties. Although fluorophores have not strictly common properties, all the fluorophores have planar structures and conjugated systems. 2,3-bis((E)-(4-(diethylamino)-2 hydroxybenzylidene) amino) maleonitrile (**1**) is an example as a fluorophore (Figure 1.3) [26]. The quantum yield of **1** in acetonitrile is Φ= 0.80 [27].

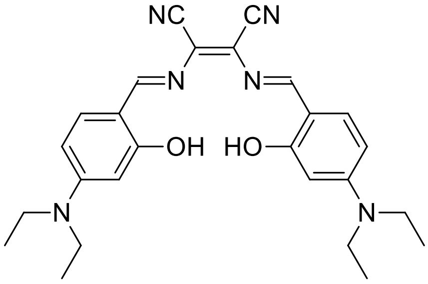

1

Figure 1.3. Molecular structure of **1**.

1.2. Aggregation Caused Quenching (ACQ)

Recently, researchers have invested a lot of effort into design and synthesis of novel florescent materials. Many of the produced materials have rigid and planar structures to render enhanced conjugation. However, many of these planar systems undergo a phenomenon known as aggregation-caused quenching (ACQ) [28]. Luminescence property of the system is weakened at high concentrated solutions or in solid form due to quenching of florescence emission. This effect limits the scope of the technological applications of organic luminescent materials [2-10].

As an example, mentioned above, **1** is highly fluorescent in dilute solutions. It shows a great fluorescence at 618 nm when excited at 540 nm [27]. On the other hand, the ACQ effect is clearly observed in different MeCN/water fractions, due to low solubility and it has been also proved by its fluorescence measurements (Figure 1.4) [26].

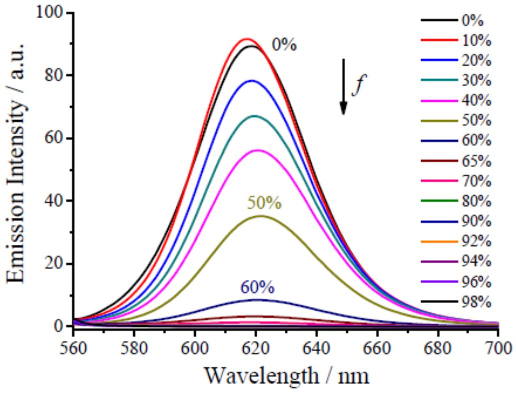

Figure 1.4. Emission spectra of **1** excited at 540 nm.

1.3. Aggregation Induced Emission (AIE)

In 2001, Tang and his co-workers opened a new era in fluorescence [29]. They synthesized 1-methyl-1,2,3,4,5-pentaphenyl-1H-silole (**2**) for highly emissive linear and hyperbranched polymers (Figure 1.5). During the purification process of **2**, they realized that the molecule has an intriguing property. The drop of compound **2**, which was dissolved in ethanol, on a TLC plate can be hardly seen under the UV light but after the solvent evaporation, the mark on the TLC plate became highly emissive. Therefore, Tang and his co-workers started to study with compound **2** in solid state and also in aggregated form. The quantum yield of PPS in ethanol ϕ_s= 0.63 x 10^{-3}, but when the solution starts to aggregate in ethanol water mixture the quantum yield of **2** in 90% water/ethanol solution ϕ_a= 0.21. The comparison between quantum yields of **2** reveals that the aggregated form is 333 times higher than in solution phase. In the light of these experiments, they came up with a whole new term called aggregation induced emission (AIE). The discovery of AIE or aggregation-enhanced emission (AEE) opens a new avenue to solve aggregation caused quenching and offers opportunities to develop new useful luminescent materials [30,31]. The AIE luminophores display non-emission in the isolated state, while highly emissive in the aggregate state. The mechanistic understanding of the AIE process has currently shown that intramolecular motions such as vibrations or rotations deactivate radiative pathways in the solution state, making the molecule non-emissive. In contrast, the restriction of intramolecular motion (RIM) in the aggregate or solid state due to physical constraints blocks non-radiative decay and boosts radiative transition. Construction of the highly efficient luminescent systems with the desired chemical and physical properties have still appealing goal for many researchers.

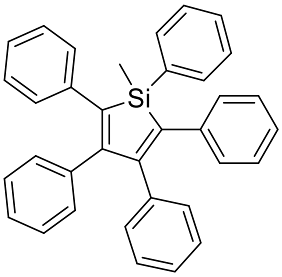

2

Figure 1.5. Molecular structure of **2**.

1.3.1. AIE luminogens (AIEgens) Systems

The current understanding of this luminescence has given rise to development of new emissive scaffolds with great structural diversity [31]. These structural features lead to categorization of these AIEgens.

1.3.1.1. Heteroatom-containing Luminogens

Compound **2** is an example of heteroatom containing luminogens. The AIE color palette of heteroatom- containing luminogens can be varied from blue to red. The main idea in the synthesis of these type of luminogens is, generating a donor-acceptor groups in the molecule and experiencing the shifts in emission spectra.

As an example, 2,3,5,6-tetraphenylpyrazine (**3**) is a heteroatom containing luminogen which will be discussed below.

1.3.1.1.1. Tetraphenyl pyrazine

Recently, it is reported that compound **3** has an aggregation induced emission feature with a high quantum yield (Figure 1.6) [32]. Compound **3**, which is heteroatom containing luminogen type, can be easily prepared under mild conditions and becomes highly emissive in aggregated state. The molecule shows a great photostability as well as thermal stability.

Pyrazine ring resides in the center of the molecule as a good electron withdrawing group, with the peripheral phenyl rings the conjugation of the molecule becomes higher due to donor-acceptor relation which is resulted with the increase in the intensity of emission bands.

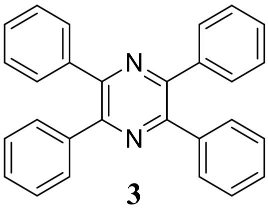

3

Figure 1.6. Molecular structure of **3**.

1.3.1.2. Luminogens with cyano Substituents

Although the cyano substituted luminogens are heteroatom- containing luminogens, these luminogens are explained as a different type AIEgen due to their enchanting properties. Possessing a high polarizability and basic structure, these type of luminogens are highly common in optical materials. (2Z,2'Z)-3,3'-([1,1':4',1''-terphenyl]-2',5'-diyl) bis(2-phenylacrylonitrile) (**4**) is an example of cyano substituted luminogen (Figure 1.7) [33]. In this example, both steric and electronic effect have an impact on the emission process. Furthermore, between these explained effects, molecule also encounters a hydrogen bonding between C-H····N in aggregated form. This situation enhances the AIE property of the molecule. Another extraordinary property about cyano substituted luminogens is, the color range can be changed by switching the position of the cyano group in molecule.

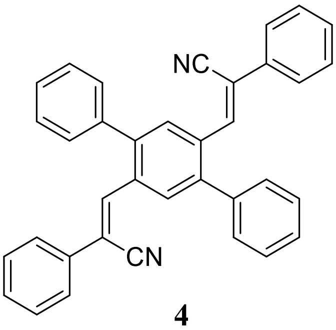

4

Figure 1.7. Molecular structure of **4**.

1.3.1.3. Hydrocarbon Luminogens

Hydrocarbon luminogens are purely consist of carbon and hydrogen and generally give an emission in blue color. (8R,8aR)-1,2,3,8,8a-pentaphenyl-8, 8a-hydrocyclopenta[a]indene (**5**) can be given as an example of hydrogen luminogens (Figure 1.8) [34]. This molecule is neutral and shows no donor-acceptor relationship between the substituents. In solution phase, the molecule experienced the intramolecular rotations. Thus, this situation leads to the attenuation of the radiative channel in emission pathway. In contrast, in aggregated form due to restriction of intramolecular rotations (RIM), it renders its emission pathway to the radiative channel and molecule starts to give an emission.

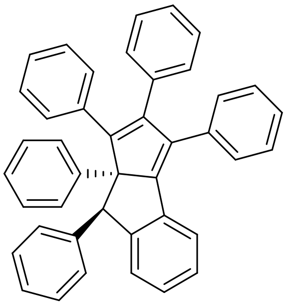

5

Figure 1.8. Molecular structure of **5**.

1.3.1.4. Luminogens with Hydrogen Bonds

In photophysics, it has been observed that the hydrogen bond formation between luminogens can stiffen the molecular structures and also activates the restriction of intramolecular rotations (RIR). As an example, in gelation process, hydrogen bonding plays a vital role. N,N'-([1,1':4',1''-terphenyl]-4,4''-diyl)bis(3,5-bis(dodecyloxy)benzamide) (**6**) were synthesized by Bo and his co-workers and in gelation process they realized that collegial effect of some non-covalent forces, including hydrogen bond formation, locked the intramolecular motion and enhances the radiative emission (Figure 1.9) [35]. This process is named as gelation induced emission and found by Park and his co-workers in 2004 [31].

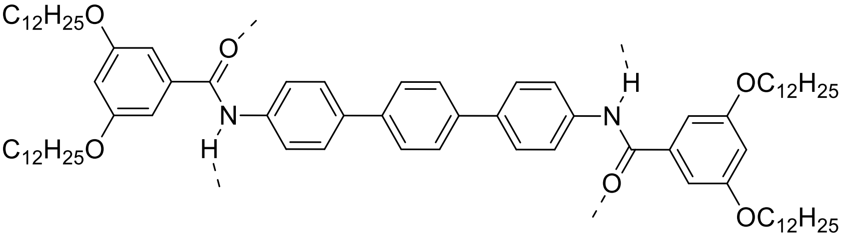

6

Figure 1.9. Molecular structure of **6**.

1.3.1.5. Luminogens without Regular Chromophores

During the purification process of 1,1,2,2-tetraphenylethene (**7**), Tang and his co-workers realized a by-product which was isolated after chromatographic separation [36]. 1,1,2,2-tetraphenylethane (**8**) was obtained as a by-product (Figure 1.10). The fluorescence measurements of **8** were carried out both in solution and in aggregated form and a weak emission curve was recognized. However, the crystals of compound **8**, showed an intense emission peak at 456 nm and this phenomenon was named as crystallization induced emission (CIE).

The exact reason why compound **8** shows an CIE property is still unknown.

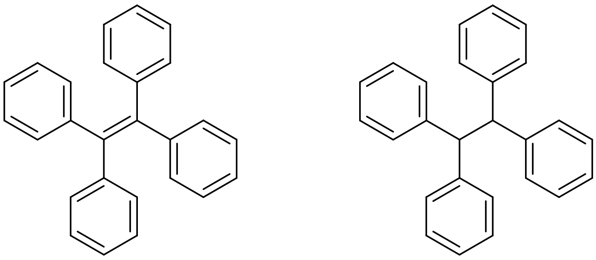

7 **8**

Figure 1.10. Molecular structure of **7** & **8**.

1.3.1.6. Polymeric Luminogens

A series of conjugated polymers that achieve enhanced light emission in the solid state have been reported in recent years (Figure 1.11) [37]. In polymeric systems, the intramolecular rotations are partly restricted because of the steric effect of the polymer chains. This is the reason why they show aggregation enhanced emission (AEE) instead of aggregation induced emission (AIE) property. As an example, compound **9** gives a weak emission in solution. However, its nanoaggregates emission is almost 20 times higher than its solution form.

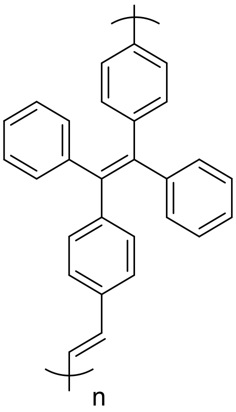

9

Figure 1.11. Molecular structure of **9**.

1.3.1.7. Organometallic Luminogens

In organic luminogenic systems, the fluorescence emission is from singlet excited state. On the other hand, in organometallic luminogens aggregation induced phosphorescence is observed and the phosphorescence emission is from triplet excited state. Compound **10** is an example for organometallic luminogen (Figure 1.12) [38]. It aggregates more efficiently in water than in organic solvents. It is assumed that intramolecular hydrophobic folding of compound **10** in aqueous medium is the reason for that solvatochromic phosphorescence.

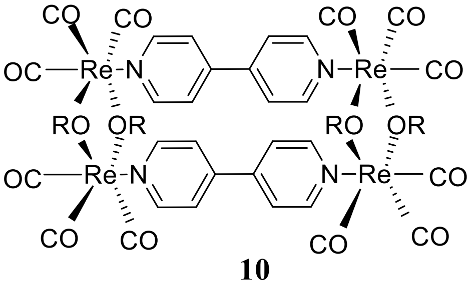

10

Figure 1.12. Molecular structure of **10**.

1.4. 2,3,5,6-tetraphenyl-1,4-dioxine

Six-membered heterocycle rings like 2,3,5,6-tetraphenyl-1,4-dioxine (**11**), drew the attention of many scientist decades ago. The significant feature of this system is, it has an eight-electron system [39]. Compound **11** has known for decades but in fact there were some conflicts about the synthesis of the molecule [40]. In 1959, Berger and Summerbell found the synthesis of **11**, by using benzoin as a starting material and followed with the addition of p-toluene sulfonic acid in catalytic amount. After some purification methods, it was obtained as a precipitate with 8% yield [41]. On the other hand, in 1964 Jerumanis and Lalancette came up with the new synthesis method for **11**, by using methyl benzoate as a starting material and continued with the addition of boron sulfide. The procedure was followed with some crystallization methods and claimed that **11** was obtained as a product [42]. However, in 1978, Yager and Wootan tried to figure out the discrepancies in these two methods and realized that; actual synthesis of **11** was achieved by Berger and Summerbell, while Jerumanis and Lalancette synthesized tetraphenyl thiophene. This error was due to incorrect elemental analysis according to Yager and Wootan. In 1985, Adam, Platsch and Schmidt offer a new synthesis method for compound **11**, which consists of two steps. First step is the formation of mono- and di-methoxy substituted dimers and the second step is the formation of the crystals of compound **11** [43].

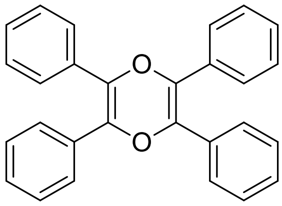

11

Figure 1.13. Molecular structure of **11**.

1.4.1. Structural Studies on Similar Dioxin Derivatives

In 2000, Mamedov and his co-workers investigated the structure of some dioxin derivatives by X-Ray analysis [44]. They offered two dioxin derivatives as dimethyl 3,5-diphenyl-1,4-dioxine-2,6-dicarboxylate (**13**) (Figure 1.14) and dimethyl 3,6-diphenyl-1,4-dioxine-2,5-dicarboxylate (**12**) (Figure 1.15).

Compound **12** has a planar dioxin ring and double bonds in this endocycle are somehow elongated. Also, the C-O bonds in dioxin ring are also longer than any other $C_{sp}{}^{2}$- O bonds in six membered heterocycle rings according to Cambridge Structural Database System (CSDS). The dihedral angles of the substituted phenyl rings and methyl ester groups are 70.2° and 3.5° with the plane dioxin core respectively. In addition, they also found out that; there is not any intramolecular contacts in **12** crystals (Figure 1.16). In contrast, **13** has both intramolecular and intermolecular contacts. The most important difference between these two dioxin derivatives are; when compound **12** has a planar core, the dioxin ring in compound **13** has a boat conformation (Figure 1.17). **13** has a reasonable symmetry plane which goes through the “O” atoms of the dioxin. The double bonds in the dioxin ring of **13** are shorter than they are in **12**. The conjugation in compound **12** is more likely between the planar dioxin core, carbonyl group of the methyl ester group and the lone pairs of “O” atom in endocyclic ring whereas conjugation in **13** is infeasible due to nonplanar structure of the dioxin.

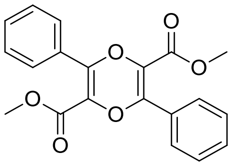

Figure 1.14. Molecular structure of **12**.

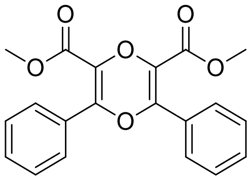

Figure 1.15. Molecular structure of **13**.

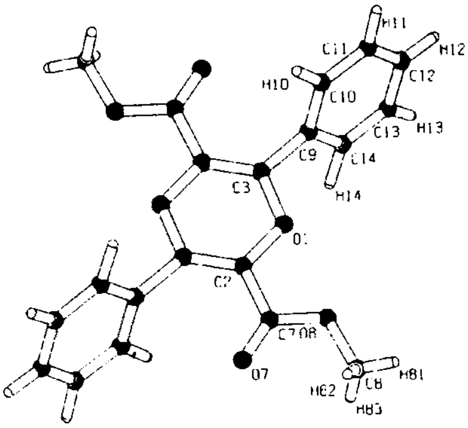

*Figure 1.16. Crystal structure of **12**.*

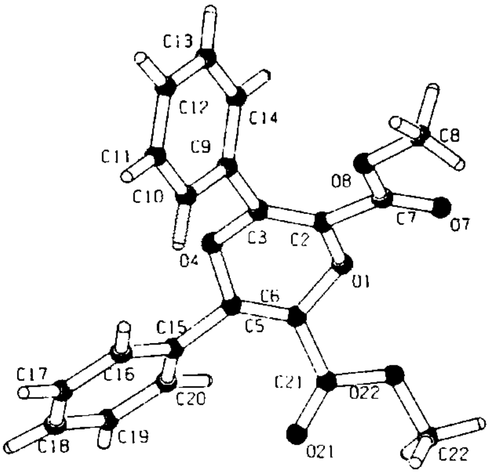

Figure 1.17. Crystal structure of **13**.

1.5. Electrochromic Devices

Electrochromic materials have reversible or irreversible electrochemical changes. These changes are due to oxidation and reduction of the materials. In electrochromic devices, the color or transmittance can be tuned through the application of voltage [45].

Electrochromic device can be divided into three parts according to their materials. These are organic small molecules, inorganics and organic polymer molecules [46].

1.5.1. Organic Polymer Molecules

Organic electronic polymers consist of highly conjugated systems. These systems are highly stable and flexible. On the other hand, due to their aromatic structures, these organic molecules cannot be easily processable. Thus, they must be polymerized to be used as an electrochromic device [47].

These systems can show multiple colors with good coloration efficiency by using same compound under different situations [48]. In 2005, this phenomenon was altered with slight modification.

Inspired from AIE property, Chen and his co-worker fabricated an electrochromic device from 1,1,2,2-tetraphenylethene (**7**), which shows electrochromic switching and fluorescence switching synchronously [49].

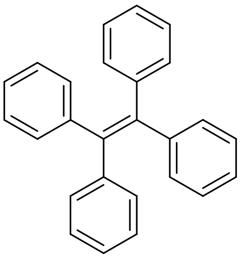

7

Figure 1.18. Molecular structure of compound **7**.

1.6. Perovskite Solar Cells

Currently, new types of renewable energy sources are highly demanded due to limited fossil fuel reserves and a rapid increase in energy need. Sunlight is the most abundant and renewable energy source. In the light of this knowledge, many photovoltaic devices have been developed to harvest the sunlight. Among all these photovoltaic devices, perovskite solar cells have attracted many scientists due to their excellent lifetime, charge-carrier mobilities and light absorption [50].

Perovskite solar cells consist of basically 5 parts (Figure 1.19).

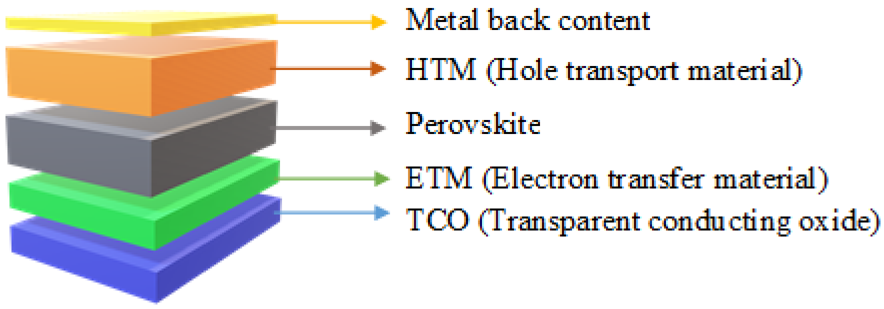

Figure 1.19. Regular perovskite solar cell diagram.

TCO is covered with electron transfer material which generates the second layer of perovskite. Generally, alumina (Al_2O_3) or combination of compact titania (TiO_2) and mesoporous TiO_2 are used as an electron transfer material (ETM) [51]. This layer is the anode side of the cell and generates a charge carrier system for electrons. Perovskite layer is placed in the middle of the cell and harvests the sunlight. The layer forms an intrinsic area in the cell. In other words, it is responsible for charge carrier between the two ends of the cell [52].

Basically, perovskite material has ABX_3 structure. While A and B refers a cation, X refers to an anion. Generally, larger cations are used as A. Methyl ammonium

($CH_3NH_3^+$), ethyl ammonium ($CH_3CH_2NH_3^+$) and formamidinium ($NH_2CHNH_2^+$) are the best-known examples of A [53]. B cations can be lead (Pb) or tin (Sn), but oxidation of Pb possesses a problem that causes a threat of the stability of a solar cell and it is toxic for environment and human health [54]. X can be halide or mixture of halides, like chloride (Cl^-), bromide (Br^-) or Iodide (I^-) or can be mixture of these anions [53]. Hole transport material (HTM) as a fourth layer of perovskite solar cell, responsible for charge carrier like ETM. Spiro-OMeTAD (**14**) and semiconducting polymers like poly(3-hexylthiphene) (P3HT) and poly(triarylamine) (PTAA) are used as HTM in perovskite solar cells [55]. The last layer is metal back bone which acts as a counter electrode and forms the cathode side of the cell. Generally, gold (Au) and silver (Ag) are used as a metal backbone [55].

1.6.1. Spiro-OMeTAD

In 2012, Lee and Teuscher opened a new era in the production of perovskite solar cells [56]. Perovskite layer was coupled with a small organic molecule called spiro-OMeTAD (**14**) (Figure 1.20). Compound **14** was used as a transparent p-type hole transport material and mesoporous TiO_2 was used as a transparent n-type material in perovskite solar cell and device showed a power conversion efficiency with 8%.

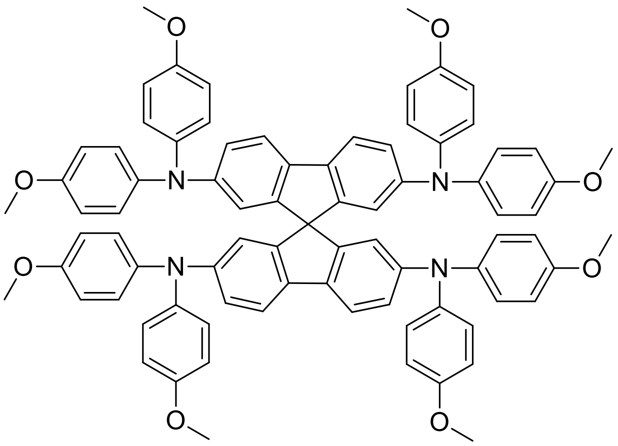

14

Figure 1.20. Molecular structure of 14.

1.7. Aim of the Study

1.7.1. Synthesis of TPD as AIE luminogen

AIE luminogens are still an on-going research since their structural diversities and unique structures, draw attention in many disciplines of science. As mentioned above, compound **3** is a new type of AIE luminogen that shows great photo-, chemo-, and thermo-stability. Besides, the synthesis of compound **3** is rather simple and efficient [32].

It can be considered that, 2,3,5,6-tetraphenyl-1,4-dioxine (**11**) has also a similar structure with **3**. Furthermore, the 3D structure of **11** was expected to be similar to propeller structure of **3**. In line with this target, the first part of the study based on the synthesis of **11** and investigation of the AIE property. The characterization of compound **11** including single crystal X-ray analysis was also performed.

1.7.2. Synthesis of TPP based Electrochromic Device

Electrochromic devices that can achieve electrochromic switching and fluorescence switching synchronously is a rare situation. In the light of this work, our second aim is to synthesize a compound **3** based polymer which will be used in electrochromic device as a film state. By doing so, we will synthesize a device which gives an electrochromic switching and fluorescence switching synchronously.

1.7.3. Synthesis of TPP based Perovskite Solar Cell

As mentioned above, spiro-OMeTAD (**14**) is used in perovskite solar cell as a hole transport material due to its non-planar structure. However, this material has some drawbacks [57]. Spiro-OMeTAD (**14**) has a long synthesis route resulting with low yield due to these reasons it has also high cost. In addition, it may be doped to be used as a hole transport material in perovskite solar cell in some cases. Still, this doping leads to a decrease in the stability of hole transport material and causes a loss in the efficiency of perovskite solar cell.

On the other hand, compound **3** based organic molecules can be an alternative way to hole transport material. Compound **3** has a non-planar structure like spiro-OMeTAD (**14**). Besides, compound **3** has a facile preparation and it has good thermo-, chemo- and photo-stability. Inspired from these features, in this study, our third motivation is to synthesize a compound **3** based hole transport material which will be used in perovskite solar cell instead of spiro-OMeTAD (**14**).

CHAPTER 2

RESULT AND DISCUSSION

2.1. Synthesis of 2,3,5,6-Tetraphenyl Dioxin (11)

In this study, first motivation is to synthesize compound **11** as a potential new type of AIE-active luminogen and performing the fluorescence measurements in different water/THF fractions. For that reason, **11** was synthesized starting from commercially available benzoin by following the literature procedure [43]. The synthesis of **11** consists of two steps. In the first step, benzoin (**15**) was dissolved in methanol and dry HCl gas was passed through the solution for 8 hours.

Dry HCl gas was formed with the reaction of sodium chloride and sulfuric acid (Scheme 2.1). Sulfuric acid was added dropwise to the sodium chloride in a sealed system. HCl gas was formed during this reaction and gas was passed through the reaction flask.

$$H_2SO_4 + 2\ NaCl \longrightarrow 2\ HCl_{(g)} + Na_2SO_4$$

Scheme 2. 1. Synthesis of dry HCl gas.

After HCl gas bubbling, the reaction was stirred at room temperature for 48 hours. At the end of the 48 hours, the precipitate was formed and filtrated with Büchner funnel and dried. The reaction resulted with the formation of dioxene and dioxane derivatives (**16**,**17**) as a white precipitate (Scheme 2.2).

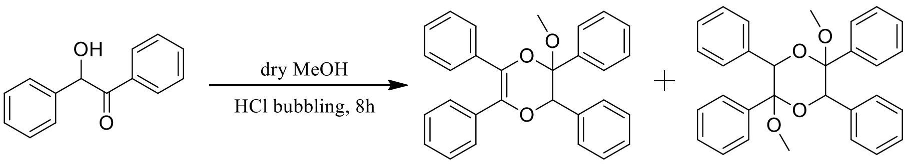

15 **16** **17**

Scheme 2. 2. Synthesis of **16** & **17**.

In the second step, the mixture of dioxene **16** and dioxane **17**, was reacted with commercially available *p*-toluenesulfonic acid in acetic anhydride under reflux for 30 minutes. The reaction was cooled to 0 °C and resulting with the formation of yellow precipitate. The solution was filtered and dried. Compound **11** was obtained as a yellow precipitate with 18% yield. The overall synthesis of **11** from benzoin (**15**) was shown below (Scheme 2.3).

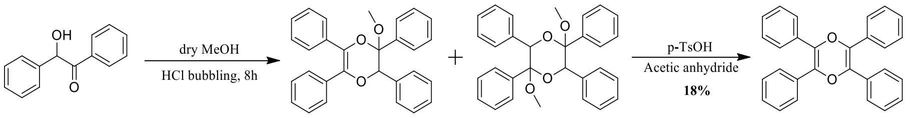

15 16 17 11

Scheme 2. 3. Overall synthesis of **11**.

2.1.1. Fluorescence Measurements of 11

After the synthesis of **11**, fluorescence measurements were performed. 1.0 x 10^{-5} M solutions of **11** were prepared in different fractions of water/THF mixtures starting from 0% to 99% water fraction in THF solution. Fluorescence spectra were recorded on Varian Cary Eclipse Fluorescence Spectrophotometer. The measurements were performed at medium voltage with a slit width of 5 nm and the solutions were excited at 375 nm. The fluorescence measurements show that **11** has an ACQ property (Figure B.2).

The quantum yield calculation of **11** was done by using commercially available anthracene as a standard due to its similar excitation and emission regions. The quantum yield of **11**, in THF solution is 0.26 while it is 0.02 in 90% water/THF mixture.

2.1.2. Crystallization of 11 & Single Crystal Analysis

Compound **11** was crystallized in toluene and petroleum ether mixture. Firstly, 11 was completely dissolved in toluene by applying a gentle heat in a heating mantle and after complete dissolution, heat was turned off. Petroleum ether was added dropwise until the solution became blurred. The solution was again gently heated until it began to boil. Then heat was turned off and the solution left 4 days in dark and remained undisturbed in a closed container. The yellow needles were obtained as a single crystal.

Single crystal analysis was performed by Assist. Prof. Ferdi Karadaş from Bilkent University (Figure 2.1). Rigaku RAXIS conversion diffractometer was used for single crystal analysis. The analysis was performed at 100 K.

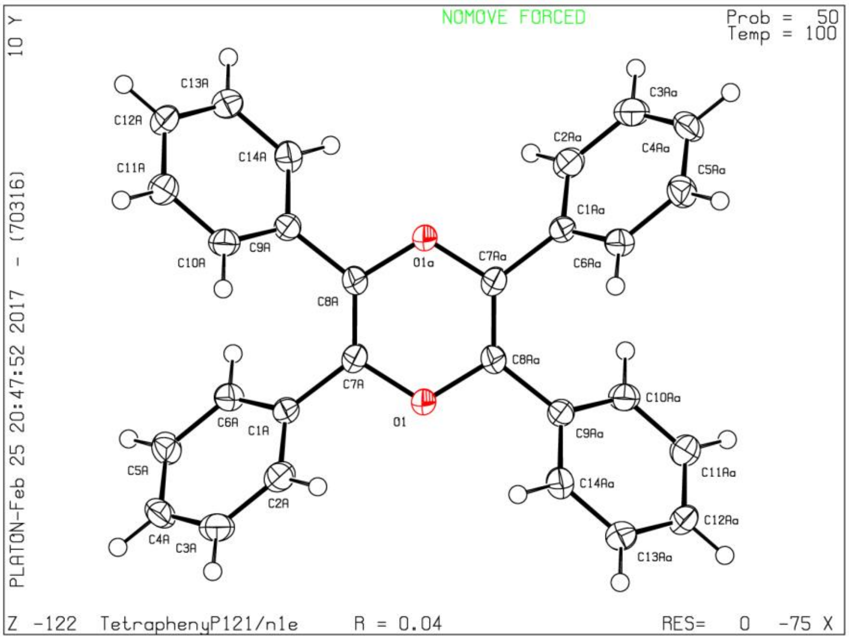

Figure 2.1. Single crystal analysis of **11**.

While the dihedral angles between C1Aa-C7Aa & C1A-C7A are 47º and C9Aa-C8Aa & C9A-C8A are 38º.

2.2. Synthesis of 2,5-bis(4-bromophenyl)-3,6-diphenylpyrazine (23)

For the synthesis of **23**, commercially available 4-Br-benzaldehyde (**18**) and benzoyl cyanide (**19**) were reacted in acetic acid with commercially available 12% aqueous $TiCl_3$ under nitrogen bubbling [58]. The resulting diol derivatives **20** and **21** were obtained as two products. Then, the mixture of these diols was reacted with potassium carbonate (K_2CO_3) in *t*-BuOH at 40 °C. 2-(4-bromophenyl)-2-hydroxy-1-phenylethanone (**22**) was obtained as a product with some impurities. Compound **22** was purified via flash column chromatography several times and due to these repeating purification processes, the yield was very low (2.7%). Compound **22** was further converted into **23** by following the literature procedure [32].

Compound **22** was reacted with ammonium acetate (NH_4OAc) in acetic acid. **23** was obtained as a product as a white solid. The overall synthesis of **23** was shown in Scheme 2.4.

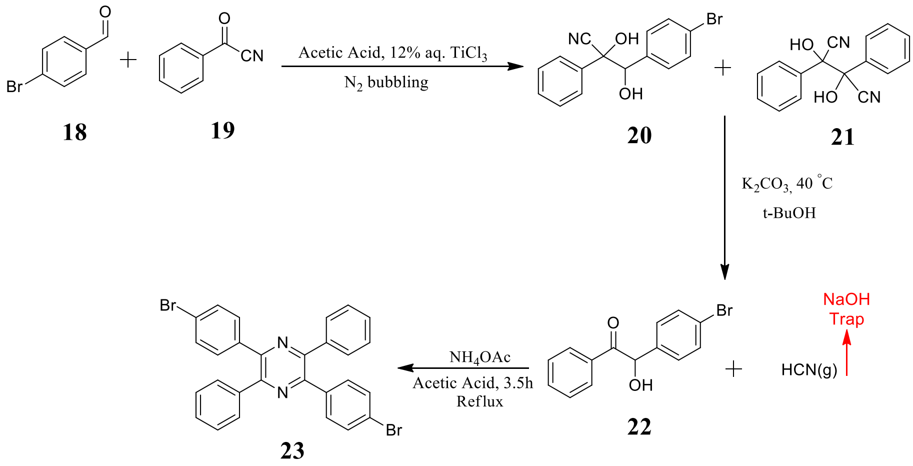

Scheme 2. 4. Overall synthesis of **23**.

2.2.1. Electrochromic Device Application of 23

Compound **23** will be polymerized with ProDOT derivative by using Pd-catalyzed coupling reactions. Tentative synthetic pathway was shown in Scheme 2.5. The product will be used in electrochromic device in film state.

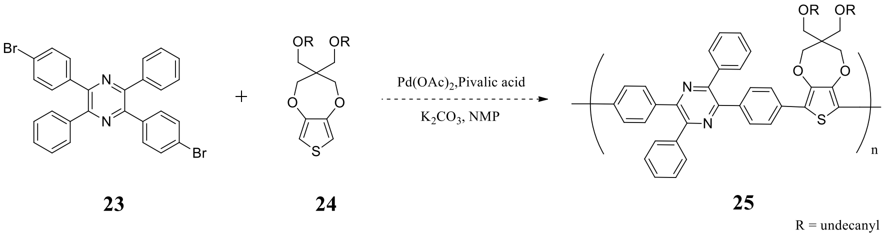

Scheme 2. 5. Synthesis of **25.**

2.2.2. Electrical properties of 25 in Electrochromic Device

Electrical properties of compound **25** as an electrochromic device will be studied by Günbaş Research group.

2.3. Synthesis of 2,3,5,6-tetrakis(4-bromophenyl) pyrazine (27)

For the synthesis of **27**, 4,4'-dibromobenzoin (**26**) was synthesized as a precursor. Starting from commercially available 4-bromo benzaldehyde (**18**), it was reacted with sodium cyanide in methanol/ water mixture by following the literature procedure [59]. and 4,4'-dibromobenzoin (**26**) was obtained as a white precipitate with good yield (72%).

Compound **26** was further reacted with ammonium acetate in acetic acid to obtain **27** as a pale-yellow precipitate with low yield (13%). ^{1}H NMR data is consistent with literature (Figure A.12 & A.13) [49]. The overall synthesis scheme was shown below (Scheme 2.6).

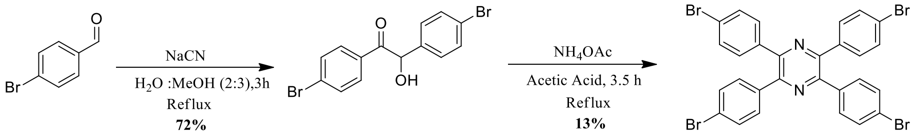

18 **26** **27**

Scheme 2. 6. Overall synthesis of **27**.

2.3.1. Crystallization& Single Crystal Analysis of 27

4Br-TPP was crystallized with vapor diffusion method. Compound **27** was dissolved in chloroform in a small vessel and placed in a larger container, which was filled with hexane. The container was tightly closed then put in dark and remained undisturbed. After 3 days, crystals of compound **27** were obtained as yellow transparent plates.

Single crystal analysis was performed by Assist. Prof. Ferdi Karadaş from Bilkent University (Figure 2.2). Rigaku RAXIS conversion diffractometer device was used for single crystal analysis. The analysis was performed at 293 K.

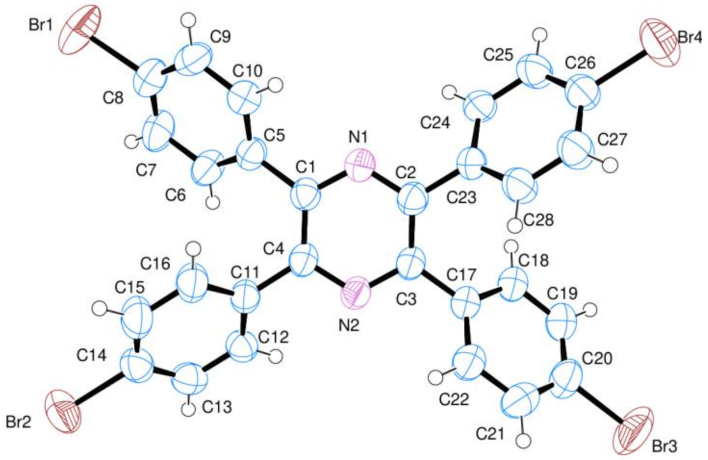

*Figure 2.2.*Single crystal of **27**.

2.3.2. Perovskite Solar Cell Application of 29 as a Hole Transport Material

Compound **27** was coupled with bis(4-methoxyphenyl)amine (**28**) via Buchwald-Hartwig coupling reaction [60]. In Buchwald-Hartwig coupling reaction, palladium acetate (Pd(OAc)$_2$) was used as a catalyst. Sodium *tert*-butoxide and tri-*tert*-butylphosphonium tetrafluoroborate were used as a base. Generally, phosphine ligands are used in Buchwald-Hartwig coupling reaction. However, the solution form is these ligands are unstable. In this study, to overcome that problem, derivative of phosphonium salt was used instead of phosphine ligands.

After the purification process, 4,4',4",4"'-(pyrazine-2,3,5,6-tetrayl)tetrakis(N,N-bis(4-methoxyphenyl)aniline) (**29**) was obtained as a product with 57% yield (Scheme 2.7). This synthesis was performed by Figen Varlıoğlu from Günbaş Research Group.

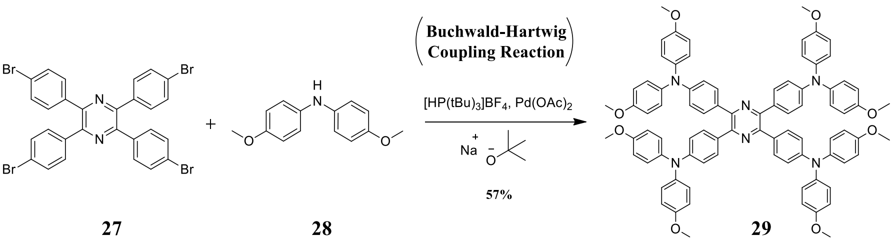

27 **28** **29**

Scheme 2. 7. Synthesis of **29**.

2.3.3. Electrical properties of 29 as Hole transport material in Perovskite Solar Cell

Electrical properties of compound **29** as a hole transport material in perovskite solar cell was done by Dr. Hava Kaya from Günbaş Research group. Optimization process will be conducted.

2.3.4. Device Fabrication of Perovskite Solar Cell

Fabrication of perovskite solar cell was done by following the literature procedure [61]. The final structure of the perovskite solar cell was shown below (Figure 2.3). The I-V characterization of the cell was investigated (Figure 2.4). The perovskite solar cell parameters are given in Table 2.1. The power conversion efficiency (PCE) was higher than reference cell. On the other hand, the short current density of compound **29** was lower than the spiro-OMeTAD case. The reason is, the perovskite cell area of compound **29** was higher than the reference cell. As a result, this characterization reveals that compound **29** has a promising result even though these results are without any optimization process.

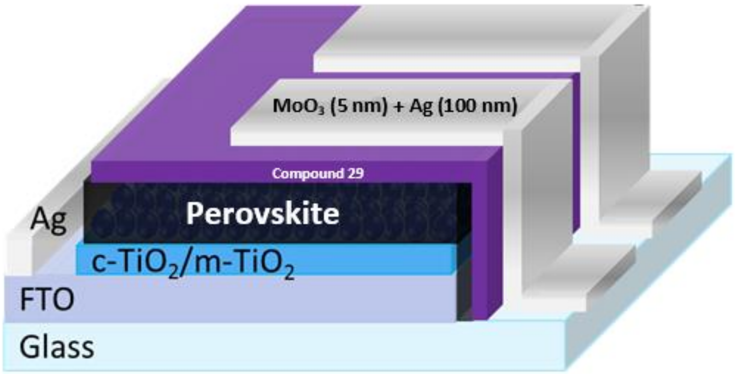

Figure 2.3. Perovskite solar cell diagram of compound **29**.

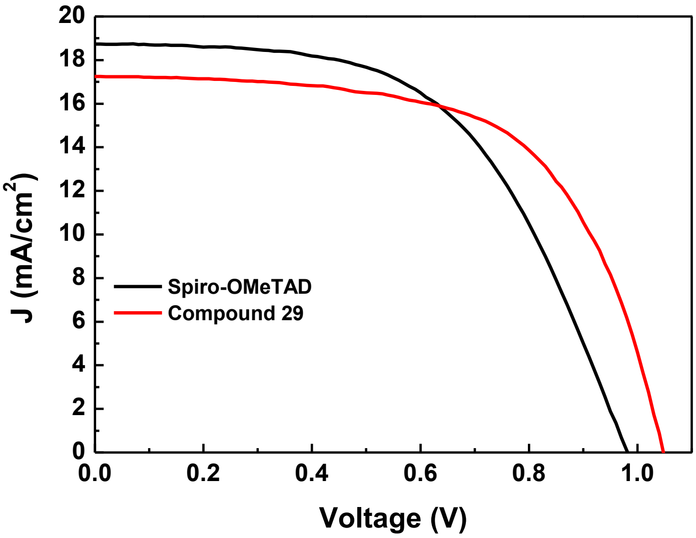

Figure 3.4. I-V characterization of compound **29** and spiro-OMeTAD.

Table 2.1. *Perovskite solar cell parameters*

	J_{sc} (mA/cm^2)	V_{oc} (V)	FF (%)	PCE (%)
Spiro-OMeTAD	18.74	0.98	55.1	10.1
Compound **29**	17.24	1.05	61.5	11.1

2.4. Conclusion

To conclude, 2,3,5,6-tetraphenyl dioxin (**11**) was synthesized and characterized successfully. The new type of fluorophore with moderate quantum yield was obtained. However, compound **11** showed an aggregation caused quenching property, instead of aggregation induced emission property. As the water fraction increases, the intensity of the emission decreases.

2,3,5,6-tetraphenyl pyrazine (**3**) was synthesized to validate the fluorescence measurements of compound **11**. Fluorescence measurements of **3** were performed and these measurements revealed that compound **3** shows an AIE property in different water/THF solutions as reported in the literature. Fluorescence measurement of **3** was shown in Appendix B.

Compound **11** was crystallized successfully and single crystal XRD measurement was performed. Crystal structure showed that it has a propeller shape and a planar core. The reason why **11** shows ACQ property, although it has a propeller shape and a planar core, will be further investigated by theoretical studies.

In the second part of the study, compound **23** was synthesized. It will be polymerized by using a Pro-dot derivative (**24**) by Günbaş research group and electrochromic device application and electrical properties will be performed as an ongoing study.

In the third part of the study, compound **27** was synthesized with low yield (13%). Then, it was coupled with bis(4-methoxyphenyl**)**amine (**28**) via Buchwald-

Hartwig reaction and 4,4',4'',4'''-(pyrazine-2,3,5,6-tetrayl)tetrakis(N,N-bis(4-methoxyphenyl)aniline) (**29**) was obtained with 57% yield. **29** was used in perovskite solar cell as a hole transport material.

CHAPTER 3

EXPERIMENTAL

3.1 Materials and Methods

4-Bromobenzaldehyde, 12% aq. $TiCl_3$, benzoin, anthracene and benzoyl cyanide were supplied from Sigma Aldrich, Germany.

Acetic acid and acetic anhydride were supplied from Sigma Aldrich, Germany.

Other solvents are technical grade. They were purified, when necessary, using distillation method.

All reactions were examined by TLC on silica gel plates and visualized by UV-light at 254 & 365 nm wavelength. Chromatographic separations were carried out by glass precoated silica gel with particle size of 0.063-0.200 mm.

Nuclear magnetic spectra were read in $CDCl_3$ on Bruker Spectrospin Advance DPX 400 spectrometer. Chemical shifts were received in parts per million (ppm) with TMS as internal reference. NMR spectra of the compounds are given in Appendix A.

Fluorescence spectra and HRMS of **11** and **29** are given in Appendix B.

Electronic properties of compound **29** are given in Appendix B. The intensity of the solar simulator was calibrated to 100mW cm^{-2} AM1.5G.

Single crystal X-ray analysis of **27** are given in Appendix C.

For lyophilization, freeze dryer, Telstar Cryodos instrument was used.

For fluorescence measurements, Varian Cary Eclipse Fluorescence Spectrophotometer was used.

3.2.Synthesis of 2,3,5,6-tetraphenyl-1,4-dioxine (11)

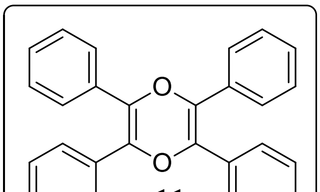

11

Benzoin (**15**) (18.5 g, 87.2 mmol) was dissolved in 140 mL methanol. Dry HCl passed through the solution for 8 hours. After 8 hours of gas bubbling, reaction was stirred for 48 hours at room temperature. The solution was filtrated via Büchner funnel and dried overnight. 8.3 g white powder was obtained as a mixture of 2-methoxy-2,3,5,6-tetraphenyl-2,3-dihydro-1,4-dioxine (**16**) and 2,5-dimethoxy-2,3,5,6-tetraphenyl-1,4-dioxane (**17**). 8.3 g white precipitate was reacted with *p*-TsOH (1.57 g, 9.12 mmol) in 27 mL dry acetic anhydride at 160 °C for 5 minutes. Reaction was allowed to cool at room temperature and placed in 0 °C ice-bath for an hour. Yellow precipitate was obtained and filtrated. Precipitate was washed with cold acetic anhydride and dried via freeze dryer. 6.08 g bright yellow precipitate was obtained as a product. Yield was 18%.

^{1}H NMR (400 MHz, $CDCl_3$) δ 7.34 – 7.27 (m, 2H), 7.19 – 7.13 (m, 3H).

^{13}C NMR (100 MHz, $CDCl_3$) δ 136.0, 132.9, 128.3, 128.2, 128.1.

HRMS $C_{28}H_{20}O_2$ [M^+]: Calculated 388.1463, found 388.1481.

3.3. Synthesis of 2,3,5,6-tetraphenylpyrazine (3)

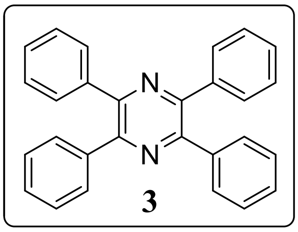

3

Benzoin (**15**) (468 mg, 1.95 mmol) was dissolved in 4 mL acetic acid. NH_4OAc (3.9 g, 5.06 mmol) was added to the solution and stirred for 3.5 hours under reflux. After 3.5 hours, reaction was allowed to cool at room temperature and precipitate was filtrated. Solid was washed with cold acetic acid and dried via freeze dryer. 285 mg white precipitate was obtained as a product. Yield is 33%.

^{1}H NMR (400 MHz, $CDCl_3$) δ 7.71 – 7.65 (m, 2H), 7.39 – 7.31 (m, 3H).

^{13}C NMR (100 MHz, $CDCl_3$) δ 148.5, 138.5, 129.9, 128.6, 128.3.

3.4. Synthesis of 2-(4-bromophenyl)-2-hydroxy-1-phenylethanone (22)

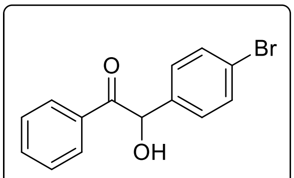

22

Bromobenzaldehyde (**18**) (3.70 g, 20.0 mmol) and benzoyl cyanide (**19**) (1.30 g, 10.0 mmol) was dissolved in 30 mL acetic acid. 28.5 mL 12% aq. $TiCl_3$ solution was added in single portion. The mixture was bubbled with N_2 bubbling at room temperature for 2 hours. Solution was extracted 5 times with 750 mL EtOAc and organic phase was collected. Then organic phase was washed with water and dried with Na_2SO_4. Solvent was evaporated under reduced pressure. 4.8 g white solid was obtained as a mixture of 3-(4-bromophenyl)-2,3-dihydroxy-2-phenylpropanenitrile (**20**) and 2,3-dihydroxy-2,3-diphenylsuccinonitrile (**21**). The white solid was dissolved in 40 mL *t*-BuOH and K_2CO_3 (1.40 g, 10.2 mmol) was added. The solution was stirred for 4 hours at 40 °C. Then 100 mL EtOAc was added and stirred for half an hour. The solution was extracted 3 times with water, organic phase was collected and dried. Solvent was evaporated under reduced pressure and 4.60 g yellow solid was obtained as a product with some impurities. The solid was purified by flash column chromatography by using different eluents on silica gel. Firstly, it was purified via flash column chromatography by using hexane, diethyl ether, chloroform mixture starting from 6:2:2 to 4:3:3 ratio respectively. 2.11 g solid was obtained and purified via flash column chromatography by using 100:1 ratio DCM:MeOH mixture. 347 mg solid was obtained and it was further purified via flash column chromatography by using a gradient solvent mixture of hexane and EtOAc (4:0 → 4:1).

78.2 mg white solid was obtained as a pure product with 2.7%. Overall synthesis **22** was shown in Scheme 8.

^{1}H NMR (400 MHz, $CDCl_3$) δ 7.88 (d, *J* = 8.5 Hz, 2H), 7.55 (s, 1H), 7.44 (s, 4H), 7.22 (s, 2H), 5.92 (s, 1H), 4.61 (s, 1H).

^{13}C NMR (100 MHz, CDCl$_3$) δ 198.51, 137.95, 134.22, 132.31, 129.43, 129.13, 128.84, 122.77, 75.44.

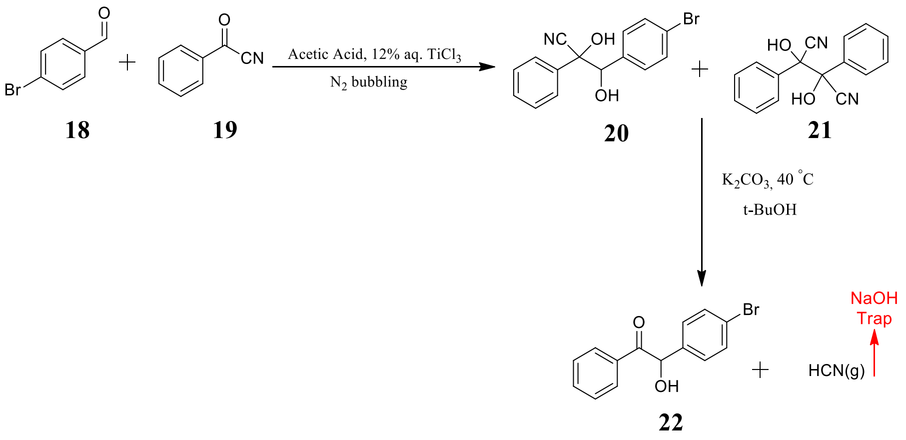

Scheme 3.1. Synthesis of **22**.

3.5. Synthesis of 2,5-bis(4-bromophenyl)-3,6-diphenylpyrazine(23)

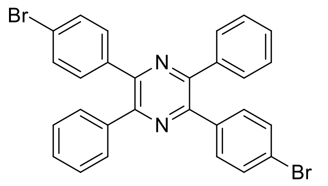

23

Compound **22** (78 mg, 0.27 mmol) was dissolved in 0.55 mL acetic acid and NH$_4$OAc (0.54 g, 0.70 mmol) was added to the solution. The reaction mixture was stirred under reflux at 160 °C for 3.5 hours. The solution was allowed to cool at room temperature and white precipitate was formed. Precipitate was filtered and washed with cold acetic acid and dried in freeze dryer. White solid was obtained with 10% yield.

^{1}H NMR (400 MHz, CDCl$_3$) δ 7.62 (s, 4H), 7.50 (s, 4H), 7.46 (s, 4H), 7.37 (s, 6H).

^{13}C NMR (100 MHz, CDCl$_3$) δ 148.6, 148.4, 147.4, 147.2, 138.0, 137.2, 131.5, 131.4, 129.8, 129.0, 128.5, 123.3.

3.6. Synthesis of 1,2-bis(4-bromophenyl)-2-hydroxyethanone (26)

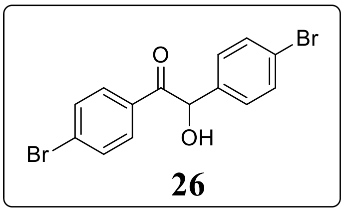

26

Compound **18** (10.0 g, 54.0 mmol) was dissolved in 12.5 mL water/methanol mixture. (2:3 ratio) NaCN (0.5 g, 10.4 mmol) was added to the solution. The reaction mixture was stirred under reflux at 110 °C for 3 hours and cooled to room temperature. Precipitate was filtered off and washed with water. 7.21 g yellow solid was obtained with 72% yield.

^{1}H NMR (400 MHz, $CDCl_3$) δ 7.77 – 7.71 (m, 2H), 7.56 (d, *J* = 7.7 Hz, 2H), 7.47 (d, *J* = 7.6 Hz, 2H), 7.19 (d, *J* = 7.7 Hz, 2H), 5.85 (d, *J* = 4.4 Hz, 1H), 4.49 (d, *J* = 5.0 Hz, 1H).

^{13}C NMR (100 MHz, $CDCl_3$) δ 197.6, 137.3, 132.4, 132.2, 132.0, 130.5, 129.6, 129.4, 123.0, 75.5.

3.7. Synthesis of 2,3,5,6-tetrakis(4-bromophenyl)pyrazine (27)

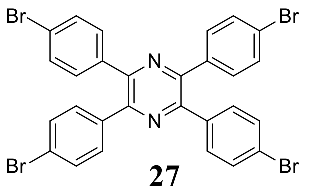

27

Compound **26** (1.92 g, 5.18 mmol) was dissolved in 10.5 mL acetic acid and NH_4OAc (10.3 g, 13.4 mmol) was added to the solution. The reaction mixture was stirred under reflux at 160 ºC for 3.5 hours. The solution was allowed to cool at room temperature and yellow precipitate was formed. Precipitate was filtered and washed with cold acetic acid and dried in freeze dryer. Pale yellow solid was obtained with 13% yield.

^{1}H NMR (400 MHz, $CDCl_3$) δ 7.49 (s, 16H).

^{13}C NMR (100 MHz, $CDCl_3$) δ 147.4, 136.7, 131.8, 131.3, 123.7.

3.8. Synthesis of compound 29

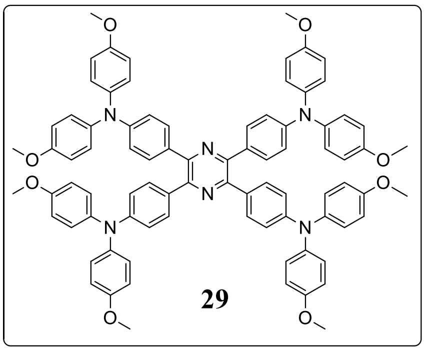

29

Compound **27** (250 mg, 0.357 mmol), bis(4-methoxyphenyl)amine (573 mg, 2.50 mmol), sodium *tert*-butoxide (203 mg, 2.11 mmol), tri-*tert*-butylphosphonium tetrafluoroborate (3.11 mg, 0.0107 mmol) and palladium (II) acetate (1.60 mg, 0.0714 mmol) were added to 50 mL Schlenk tube and vacuum/argon was applied successively. After addition of 25 mL of freshly distilled toluene, argon bubbling was performed for 30 minutes, temperature was raised to 100 °C and stirred for 48 hours. The reaction mixture was purified with 9:1 ratio hexane: EtOAc in neutral alumina. Further purification was done in neutral alumina using DCM: hexane (1:1 ratio) as an eluent and resulting yellow solid was recrystallized from DCM: hexane 1:1 ratio. Yellow solid was obtained with 57% yield.

^{1}H NMR (400 MHz, $CDCl_3$) δ 7.51 (d, *J* = 8.7 Hz, 4H), 7.09 (d, *J* = 8.9 Hz, 8H), 6.84 (m, 12H), 3.81 (s, 12H).

^{13}C NMR (101 MHz, $CDCl_3$) δ 156.0, 148.8, 146.3, 140.6, 130.6, 130.4, 126.9, 119.3, 114.7, 55.5.

HRMS $C_{84}H_{72}N_6O_2$ [M$^+$]: Calculated 1292.5412, found 1292.5438.

3.9. Device Fabrication of Perovskite Solar cell

FTO substrates were etched with Zn powder and 2M HCl solution. After the etching process, the substrates were cleaned in ultrasonic bath in 2% Hellmanex solution for 15 minutes and rinsed with deionized water. For further cleaning, the substrates were placed in ultrasonic bath and sonicated in isopropanol for 15 minutes and then sonicated in acetone for 15 minutes. In the end, substrates were cleaned under UV-Ozone for 15 minutes.

For the ETM coating;

a) c-TiO_2 layer;

0.15 M and 0.30 M TTIP solutions were prepared in *n*-butanol and 2 M HCl solution (dropwise addition) and stirred overnight. The solutions were coated 1500 rpm for 6 seconds and 3000 rpm 20 seconds respectively. The substrates were annealed for 30 minutes at 500 ºC then let them cool to room temperature. Substrates were treated with $TiCl_4$ for 45 minutes at 75 ºC and annealed at 500 ºC for 30 minutes.

b) m-TiO_2 layer;

150 mg 18NRT DyeSol titania paste was dissolved in 1 mL ethanol and spin coated at 4000 rpm for 20 seconds. Then annealed at 500 ºC for 30 minutes.

c) Li-TFSI layer;

11 mg bis(trifluoromethylsulfonyl)amine lithium salt was dissolved in 750 μL isopropanol and coated at 2000 rpm for 2 seconds and 3000 rpm for 8 seconds by spin-coating method, annealed at 500 ºC for 30 minutes.

For perovskite coating; triple cation films as a form of $FA_xMA_yCs_{1-x-y}Pb(I_z, Br_{1-z})_3$ (FAMACs) were prepared. 172 mg FAI, 507 mg PbI_2, 22.4 mg MABr, 73.4 mg $PbBr_2$, 40 μL of CsI (1.5 M in DMSO) (1:1:1:0.2:0.2 mole ratio) was dissolved in 627 mg DMF and 182 mg DMSO (4:1, v/v). The solution was coated on the substrates by spin-coating method at 1000 rpm for 10 seconds and 4000 rpm for 20 seconds respectively. While the substrate was spinning, 0.1 mL of chlorobenzene was rapidly dropped through the film with 6 seconds remaining in the spin-coating process to get a transparent orange film. The substrates were annealed for one hour at 100 ºC. Compound **29** films were deposited from a solution that contained 19.4 mg, 15 mmol of compound **29**, 6.7 μL of tBP, 6 μL of 1.8 M LiTFSI stock solution and 3.6 μL of 0.25 M FK209 stock solution were dissolved in 500 μL chlorobenzene and solution was coated on a surface at 4000 rpm for 30 seconds by spin-coating method. As a final layer, 5 nm MoO_3 and 100 nm Ag was coated as a metal back bone by thermal evaporation.

As a reference perovskite solar cell, spiro-OMeTAD was used as a hole transport material in perovskite solar cell. Spiro-OMeTAD films were deposited from a solution that contains 75 mg, 61.2 mmol spiro-OMeTAD, 27. 6 μL of tBP, 25 μL of 1.8 M LiTFSI stock solution and 15 μL of 0.25 M FK209 stock solution were dissolved in 1 mL chlorobenzene and solution was coated on a surface at 4000 rpm for 30 seconds by spin-coating method.

REFERENCES

1) Shinde, K. N.; Dhoble, S. J.; Swart, H. C.; Kyeongsoon, P. *Phosphate phosphors for solid-state lighting*. Heidelberg: Springer. **2012**, *174*, 2196-2812.

2) Spano F. C. The Spectral Signatures of Frenkel Polarons in H- and J-Aggregates. *Acc. Chem. Res.* **2010**, *43*, 429-439.

3) Luo J.; Xie Z.; Lam J. W. Y.; Cheng L.; Chen H.; Qiu C.; Kwok H. S.; Zhan X.; Liu Y.; Zhu D.; Tang B. Z. Aggregation-induced emission of 1-methyl-1,2,3,4,5-pentaphenylsilole. *Chem. Commun.* **2001**, *18*, 1740-1741.

4) Kalyani N. T.; Dhoble S. J. Organic light emitting diodes: Energy saving lighting technology—A review. *Renew. Sust. Energ Rev.*, **2012**, *16*, 2696–2723.

5) Reineke S.; Lindner F.; Schwartz G.; Seidler N.; Walzer K.; Luessem B.; Leo K. White organic light-emitting diodes with fluorescent tube efficiency. *Nature*, **2009**, *459*, 234–238.

6) Kelley T. W.; Baude P. F.; Gerlach C.; Ender D. E.; Muyres D.; Haase M. A.; Vogel D. E.; Theiss S. D. Recent Progress in Organic Electronics: Materials, Devices, and Processes. *Chem. Mater.* **2004**, *16*, 4413–4422.

7) Shen J.; Zhu Y.; Yang X.; Li C. Graphene quantum dots: emergent nanolights for bioimaging, sensors, catalysis and photovoltaic devices. *Chem. Commun.* **2012**, *48*, 3686–3699.

8) Gabe Y.; Urano Y.; Kikuchi K.; Kojima H.; Nagano T. Highly Sensitive Fluorescence Probes for Nitric Oxide Based on Boron Dipyrromethene ChromophoreRational Design of Potentially Useful Bioimaging Fluorescence Probe. *J. Am. Chem. Soc.* **2004**, *126*, 3357–3367.

9) Friend R. H.; Gymer R. W.; Holmes A. B.; Burroughes J. H.; Marks R. N.; Taliani C.; Bradley D. D. C.; Dos Santos D. A.; Bredas J. L.; Logdlund M.; Salaneck W. R. Electroluminescence in conjugated polymers. *Nature*. **1999**, *397*, 121-128.

10) Cornil J.; Beljonne D.; Calbert J. P.; Br´edas J. L. Interchain Interactions in Organic π-Conjugated Materials: Impact on Electronic Structure, Optical Response, and Charge Transport. *Adv. Mater.* **2001**, *13*, 1053-1067.

11) Chen Q.; Fang H.; Xu B.; Yang J.; Xia H.; Chen F., Tian W.; Sun H. Two-photon induced amplified spontaneous emission from needlelike triphenylamine-containing derivative crystals with low threshold. *Appl. Phys. Lett.* **2009**, *94*, 201113.

12) Varghese S.; Das S. Role of Molecular Packing in Determining Solid-State Optical Properties of π-Conjugated Materials. *J. Phys. Chem. Lett.* **2011**, *2*, 863-873.

13) Hu R.; Leung N. L. C.; Tang B. Z. AIE macromolecules: syntheses, structures and functionalities. *Chem. Soc. Rev.* **2014**, *43*, 4494-4562.

14) Liang J.; Tang B. Z.; Liu B. Specific light-up bioprobes based on AIEgen conjugates. *Chem. Soc. Rev.* **2015**, *44*, 2798-2811.

15) Harvey E. N. *A history of luminescence: From the earliest times until 1900*. Dover Publications, **2005**.

16) Godbey, W. T. *An Introduction to Biotechnology: The Science, Technology and Medical Applications.* Academic Press, **2014**.

17) Becker R. S. *Theory and interpretation of fluorescence and phosphorescence.* Wiley Interscience, **1969**.

18) Moretti C.; Tao X.; Koehl, L.; Koncar V. *Smart Textiles and their Applications.* Woodhead Publishing, **2016**, 539-568.

19) Zink J. I. Triboluminescence. *Acc. Chem. Res.* **1978** ,*11*, 289-295.

20) Putterman, S. J. Sonoluminescence: sound into light. *Sci. Am.* **1995**, *272*, 46-51.

21) Weiser, H. B. Crystalloluminescence. *J. Phys. Chem. C,* **1918**, *22*, 480-509.

22) Moldoveanu S. C.; David V. *Selection of the HPLC method in chemical analysis*. Elsevier, **2016**.

23) Thouand G.; Marks R. *Bioluminescence: Fundamentals and Applications in Biotechnology*. Springer, **2014**.

24) Yen W. M.; Yamamoto H. *Fundamentals of phosphors*. CRC Press, **2006**.

25) Bos A. J. J. Theory of thermoluminescence. *Radiat. Meas.* **2006**, *41*, 45-56.

26) Cheng J.; Wei K.; Ma X.; Zhou X.; Xiang H. Synthesis and photophysical properties of colorful salen-type Schiff bases. *J. Phys. Chem. C*, **2013**, *117*, 16552-16563.

27) Ma X.; Sun R.; Cheng J.; Liu J.; Gou F.; Xiang H.; Zhou X. Fluorescence aggregation-caused quenching versus aggregation-induced emission: A visual teaching technology for undergraduate chemistry students. *J. Chem. Educ.* **2015**, *93*, 345-350.

28) Birks J. B. *Photophysics of aromatic molecules*. Wiley Interscience, **1970**.

29) Luo J.; Xie Z.; Lam J. W.; Cheng L.; Chen H.; Qiu C.; Tang B. Z. Aggregation-induced emission of 1-methyl-1, 2, 3, 4, 5-pentaphenylsilole. *Chem. Commun.* **2001**, *18*, 1740-1741.

30) Viglianti L.; Leung N. L.; Xie N.; Gu, X.; Sung H. H.; Miao Q.; Tang B. Z. Aggregation-induced emission: mechanistic study of the clusteroluminescence of tetrathienylethene. *Chem. Sci.* **2017**, *8*, 2629-2639.

31) Hong Y.; Lam J. W. Y.; Tang B. Z. Aggregation Induced Emission. *Chem. Soc. Rev*. **2011**, *40*, 5361-5388.

32) Chen M.; Li L.; Nie H.; Tong J.; Yan L.; Xu B.; Tang B. Z. Tetraphenylpyrazine-based AIEgens: facile preparation and tunable light emission. *Chem. Sci.* **2015**, *6*, 1932-1937.

33) Li Y.; Li F.; Zhang H.; Xie Z.; Xie W.; Xu H.; Li B.; Shen F.; Ye L.; Hanif M.; Ma D.; Ma Y.; Tight intermolecular packing through supramolecular interactions in crystals of cyano substituted oligo(para-phenylene vinylene): a key factor for aggregation-induced emission. *Chem. Commun.* **2007**, *3*, 231-233.

34) Wu Y. T.; Kuo M. Y.; Chang Y. T.; Shin C. C.; Wu T. C.; Tai C. C.; Cheng T. H.; Liu W. S. Synthesis, structure, and photophysical properties of highly substituted 8,8a-dihydrocyclopenta[a]indenes. *Angew. Chem. Int. Ed.* **2008**, *47*, 9891.

35) Chen Y.; Lv Y.; Han Y.; Zhu B.; Zhang F.; Bo Z.; Liu C. Y. Dendritic Effect on Supramolecular Self-Assembly: Organogels with Strong Fluorescence Emission Induced by Aggregation. *Langmuir* **2009**, *25*, 8548.

36) Hong Y.; Lam J. W.; Tang B. Z. Aggregation-induced emission. *Chem. Soc. Rev.*, **2011**, *40*, 5361-5388.

37) Yuan W. Z.; Zhao H.; Shen X. Y.; Mahtab F.; Lam J. W.; Sun J. Z.; Tang B. Z. Luminogenic polyacetylenes and conjugated polyelectrolytes: synthesis, hybridization with carbon nanotubes, aggregation-induced emission, superamplification in emission quenching by explosives, and fluorescent assay for protein quantitation. *Macromolecules*. **2009**, *42*, 9400-9411.

38) Manimaran B.; Thanasekaran P.; Rajendran T. R.; Lin J.; Chang I. J.; Lee G. H.; Peng S. M.; Rajagopal S.; Lu K. L. Luminescence Enhancement Induced by Aggregation of Alkoxy-Bridged Rhenium(I) Molecular Rectangles. *Inorg. Chem.* **2002**, *41*, 5323-5325.

39) Lahiri S.; Dabral V.; Bhat V.; Jemmis E. D.; George M. V. Thermal and photochemical transformations of tetraphenyl-p-dioxin and tetraphenyl-p-dithiin. *Proc. Natl. Acad. Sci. India Sect. A.* **1977,** *86*, 1-14.

40) Yager B. J.; Wootan Jr. W. L. An investigation of discrepancies in the reported properties of tetraphenyl-p-dioxin. *Can. J. Chem.* **1978**, *56*, 1043-1044.

41) Berger D. R.; Summerbell R. K. Thermal Rearrangement of Tetraphenyl-p-dioxadiene. *J. Org. Chem.* **1959**, *24*, 1881-1883.

42) Jerumanis S.; Lalancette J. M. Réaction du Sulfure de Bore Avec Quelques Groupes Carbonyles. *Can. J. Chem.* **1964**, *42*, 1928-1935.

43) Adam W.; Platsch H.; Schmidt E. Synthesis, Thermal Stability, and Chemiluminescence Properties of Bisdioxetanes Derived from p-Dioxines. *Chem. Ber.* **1985**, *118*, 4385-4403.

44) Mamedov V. A.; Tsuboi S.; Mustakimova L. V.; Hamamoto H.; Gubaidullin A. T.; Litvinov I. A., Levin Y. A. 1, 4-dioxins from methyl phenylchloropyruvate. Competition of the Darzens, Favorskii, and Gabriel reactions. *Chem. Heterocycl. Compd.* **2000**, *36*, 911-922.

45) Sotzing G. A.; Reddinger J. L.; Katritzky A. R.; Soloducho J.; Musgrave R.; Reynolds J. R.; Steel P. J. Multiply colored electrochromic carbazole-based polymers. *Chem. Mater.* **1997**, *9*, 1578-1587.

46) Kline W. M.; Lorenzini R. G.; Sotzing G. A. A review of organic electrochromic fabric devices. *Color. Technol.* **2014**, *130*, 73-80.

47) Thompson B. C.; Kim Y. G.; McCarley T. D.; Reynolds J. R. Soluble narrow band gap and blue propylenedioxythiophene-cyanovinylene polymers as multifunctional materials for photovoltaic and electrochromic applications. *J. Am. Chem. Soc.* **2006**, *128*, 12714-12725.

48) Sonmez G.; Wudl F. Completion of the three primary colours: the final step toward plastic displays. *J. Mater. Chem.* **2005**, *15*, 20-22.

49) Chen M.; Nie H.; Song B.; Li L.; Sun J. Z.; Qin A.; Tang B. Z. Triphenylamine-functionalized tetraphenylpyrazine: facile preparation and multifaceted functionalities. *J. Mater. Chem. C*, **2016**, *4*, 2901-2908.

50) Kojima A.; Teshima K.; Shirai Y.; Miyasaka T. Organometal halide perovskites as visible-light sensitizers for photovoltaic cells. *J. Am. Chem. Soc.* **2009**, *131*, 6050-6051.

51) Kour N.; Mehra R. Recent Advances in Photovoltaic Technology based on Perovskite Solar Cell-A Review. *Int. Res. J. Eng. Technol*, **2017**, *4*, 1284-1296.

52) Taretto K.; Soldera M.; Koffman-Frischknecht A. Material parameters and perspectives for efficiency improvements in perovskite solar cells obtained by analytical modeling. *IEEE J. Photovolt.*, **2017**, *7*, 206-213.

53) Ng C. H.; Lim H. N.; Hayase S.; Zainal Z.; Huang N. M. Photovoltaic performances of mono-and mixed-halide structures for perovskite solar cell: A review. *Renew. Sust. Energ. Rev.* **2018**, *90*, 248-274.

54) Du H. J.; Wang W. C.; Zhu J. Z. Device simulation of lead-free $CH_3NH_3SnI_3$ perovskite solar cells with high efficiency. *Chin. Phys. B*. **2016**, *25*, 108802.

55) Teh C. H.; Daik R.; Lim E. L.; Yap C. C.; Ibrahim M. A.; Ludin N. A.; Teridi M. A. M. A review of organic small molecule-based hole-transporting materials for meso-structured organic–inorganic perovskite solar cells. *J. Mater. Chem. A*, **2016**, *4*, 15788-15822.

56) Lee M. M.; Teuscher J.; Miyasaka T.; Murakami T. N.; Snaith H. J. Efficient hybrid solar cells based on meso-superstructured organometal halide perovskites. *Science*. **2012**, *338*, 643-647.

57) Salim T.; Sun S.; Abe Y.; Krishna A.; Grimsdale A. C.; Lam Y. M. Perovskite-based solar cells: impact of morphology and device architecture on device performance. *J. Mater. Chem. A*, **2015**, *3*, 8943-8969.

58) Clerici A.; Porta O. Reductive coupling of benzoyl cyanide and carbonyl compounds by aqueous titanium (III) ions. A new convenient and selective access to the less stable mixed benzoins. *J. Org. Chem.*, **1993**, *58*, 2889-2893.

59) Bosiak M. J.; Trzaska P.; Kędziera D.; Adams J. Synthesis and photoluminescence properties of star-shaped 2, 3, 6, 7-tetrasubstituted benzo [1, 2-b: 4, 5-b′] difurans. *Dyes Pigm.* **2016**, *129*, 199-208.

60) Malinauskas T.; Tomkute-Luksiene D.; Sens R.; Daskeviciene M.; Send R.; Wonneberger H.; Getautis, V. Enhancing thermal stability and lifetime of solid-state dye-sensitized solar cells via molecular engineering of the hole-transporting material spiro-OMeTAD. *ACS Appl. Mater. Interfaces*, **2015**, *7*, 11107-11116.

61) Christians J. A.; Schulz P.; Tinkham J. S.; Schloemer T. H.; Harvey S. P.; De Villers B. J. T.; Luther J. M. Tailored interfaces of unencapsulated perovskite solar cells for> 1000 hour operational stability. *Nat. Energy.*, **2018**, *3*, 68-74.

APPENDICES

A. Appendix A

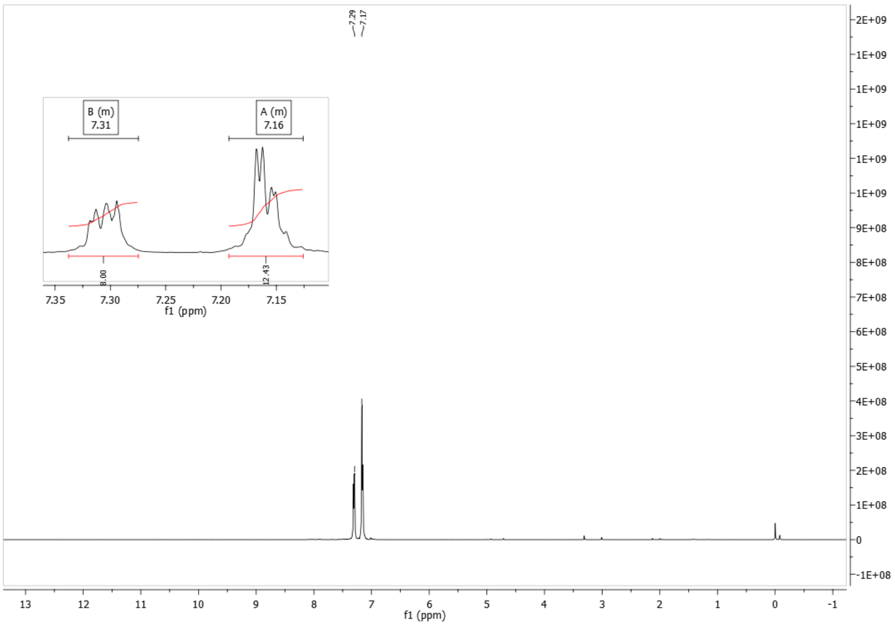

Figure A.1. ^{1}H NMR data of **11**.

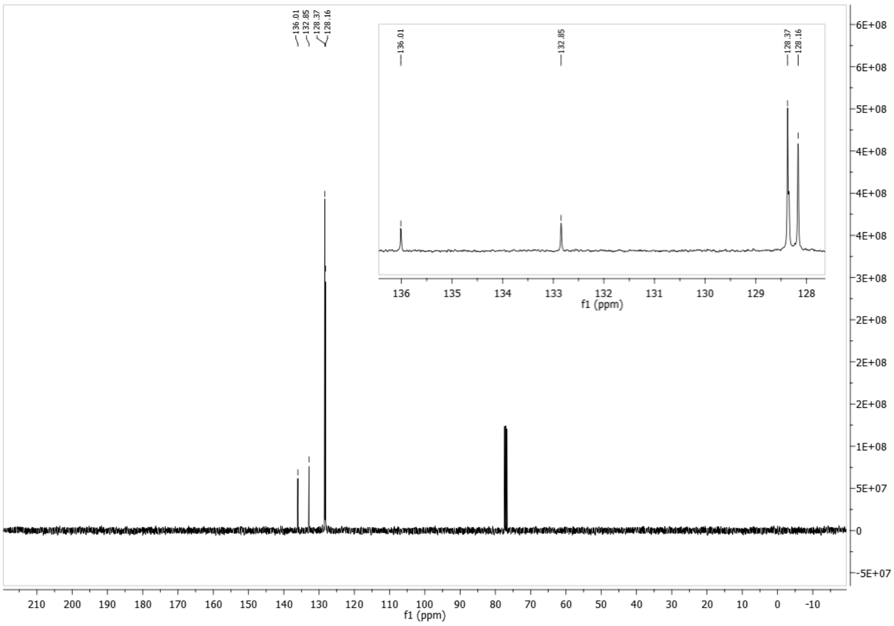

Figure A.2. ^{13}C NMR data of **11**.

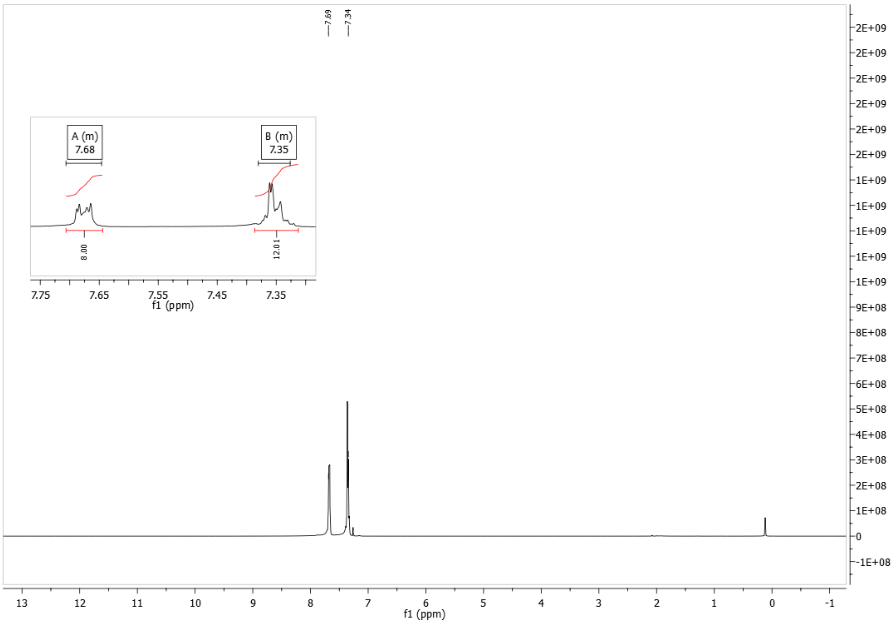

Figure A.3. ^{1}H NMR Data of **3**.

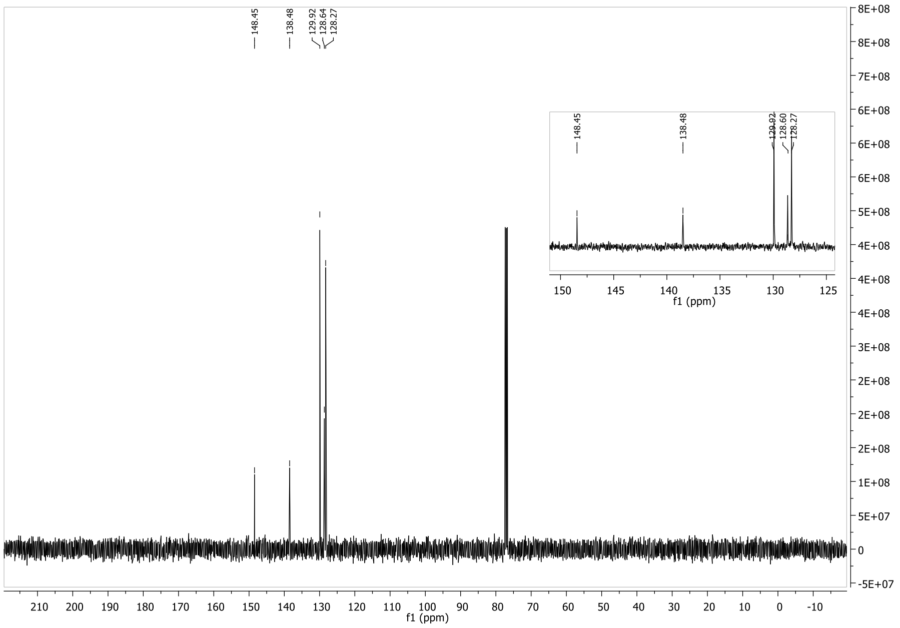

Figure A.4. ^{13}C NMR data of **3**.

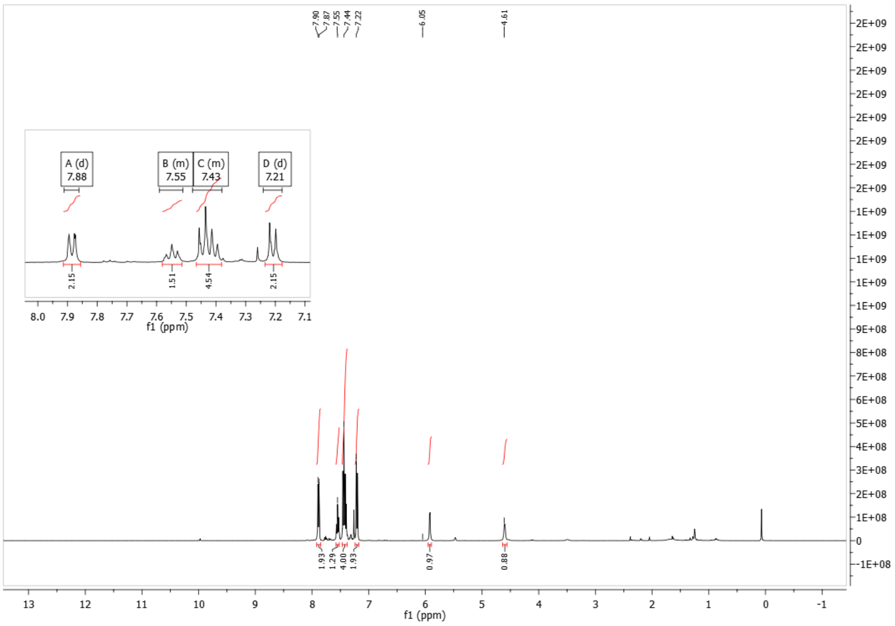

Figure A.5. ^{1}H NMR of **22**.

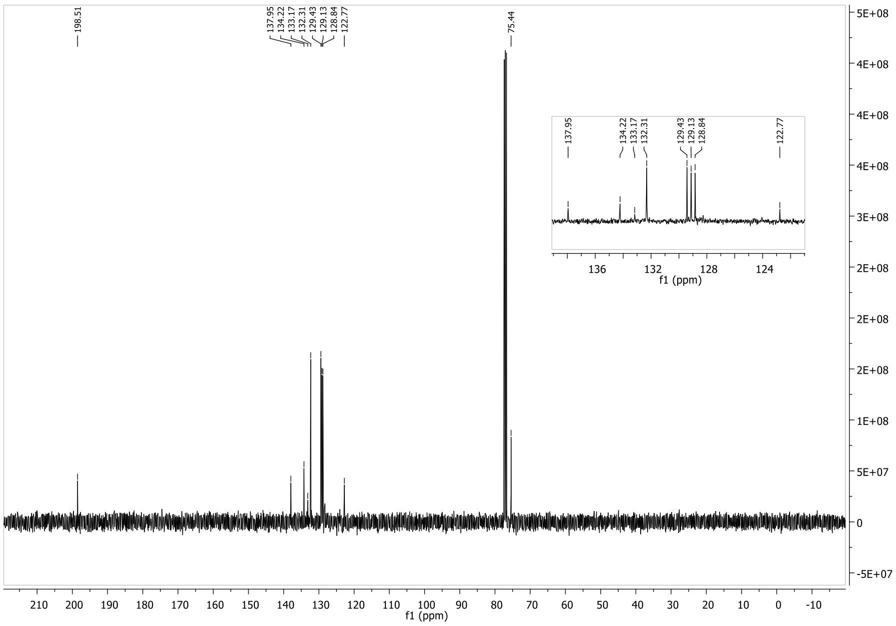

Figure A.6. ^{13}C NMR of **22**.

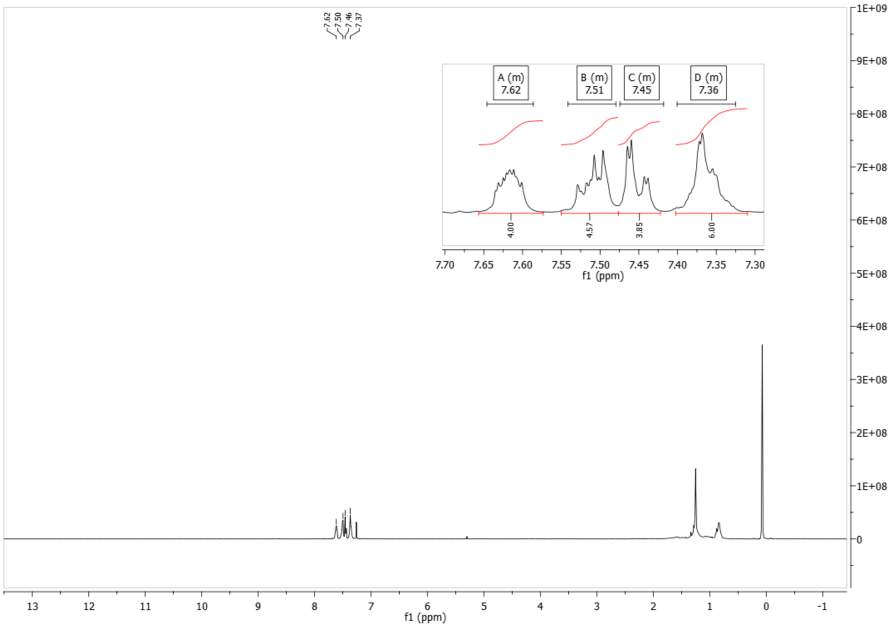

Figure A.7. ^{1}H NMR of **23**.

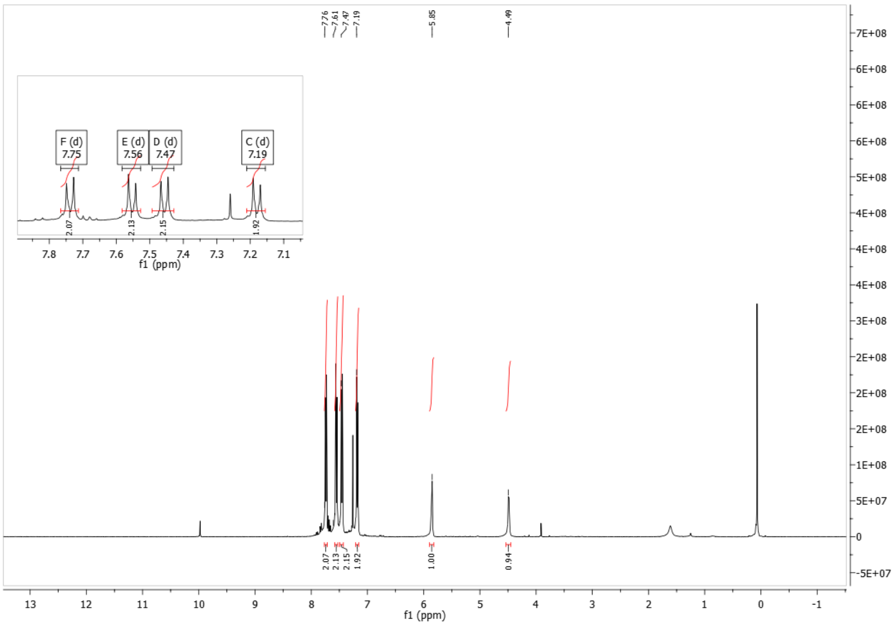

Figure A.8. ^{1}H NMR data of **26**.

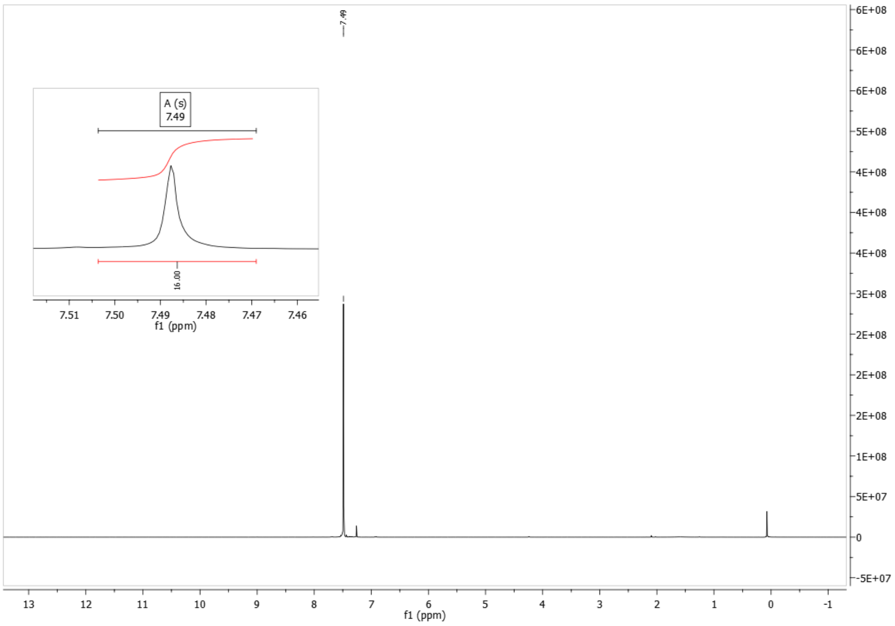

Figure A.9. ^{1}H NMR data of **27**.

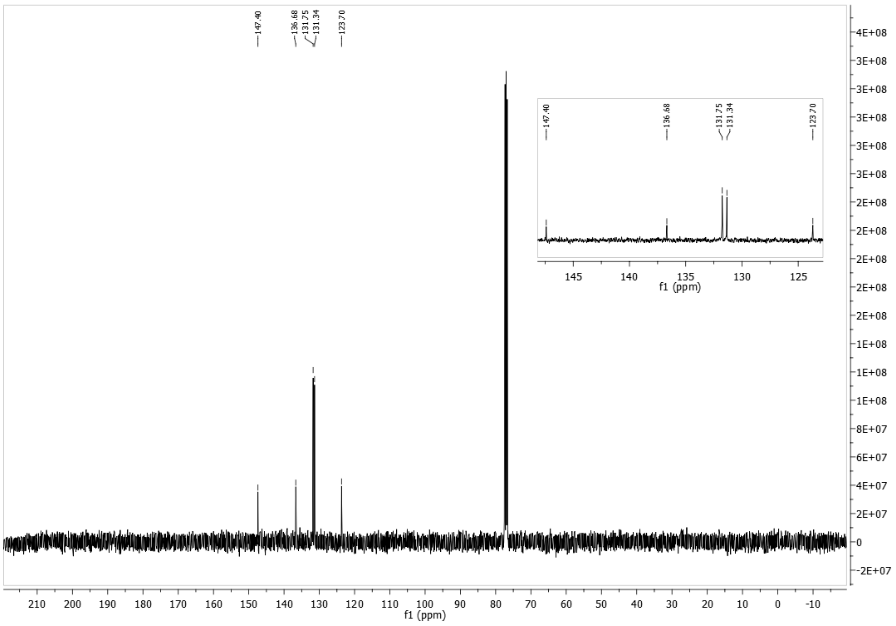

Figure A.10. ^{13}C NMR data of **27**.

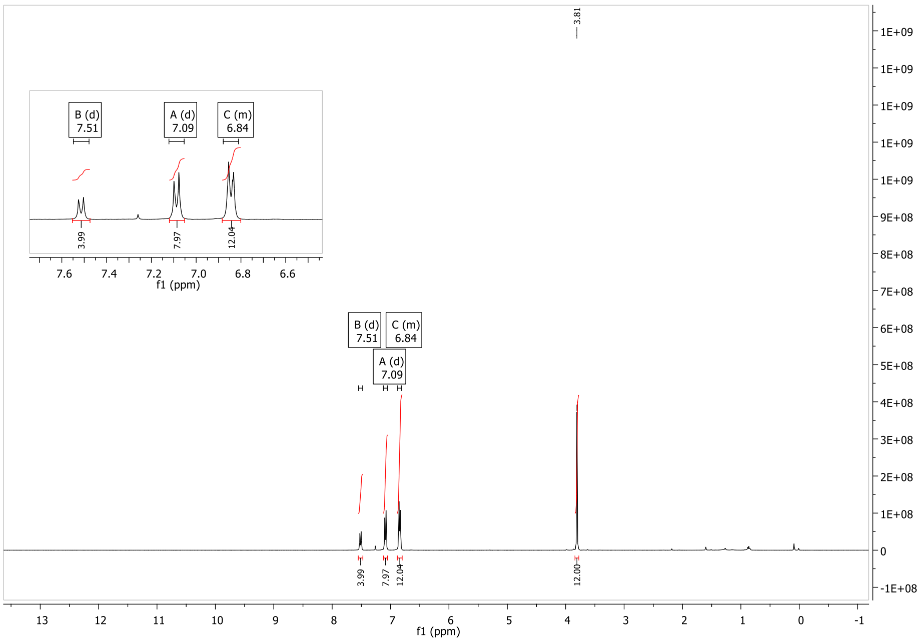

Figure A.11. ^{1}H NMR data of **29**.

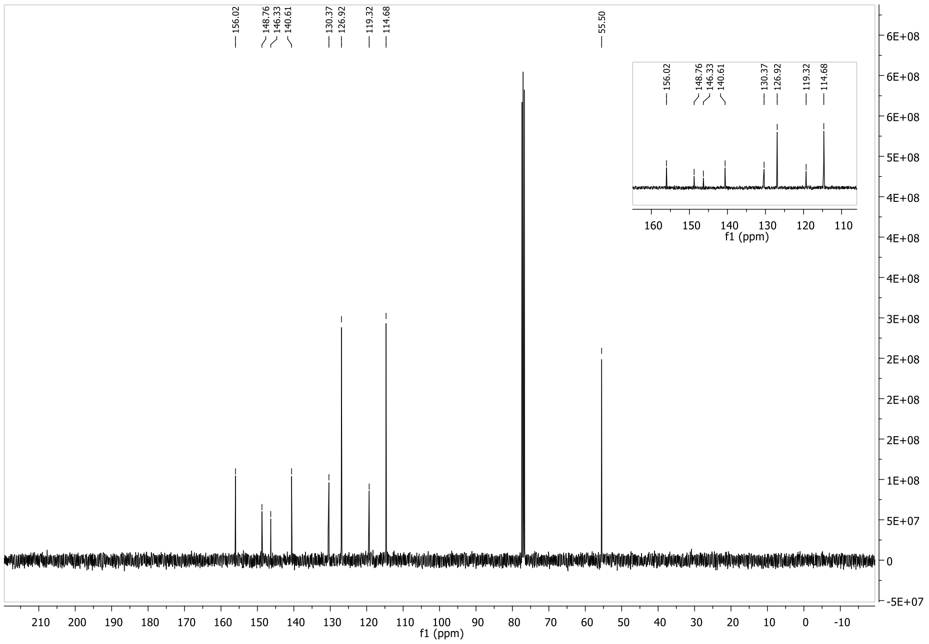

Figure A.12. ^{13}C NMR data of **29**.

B. Appendix B

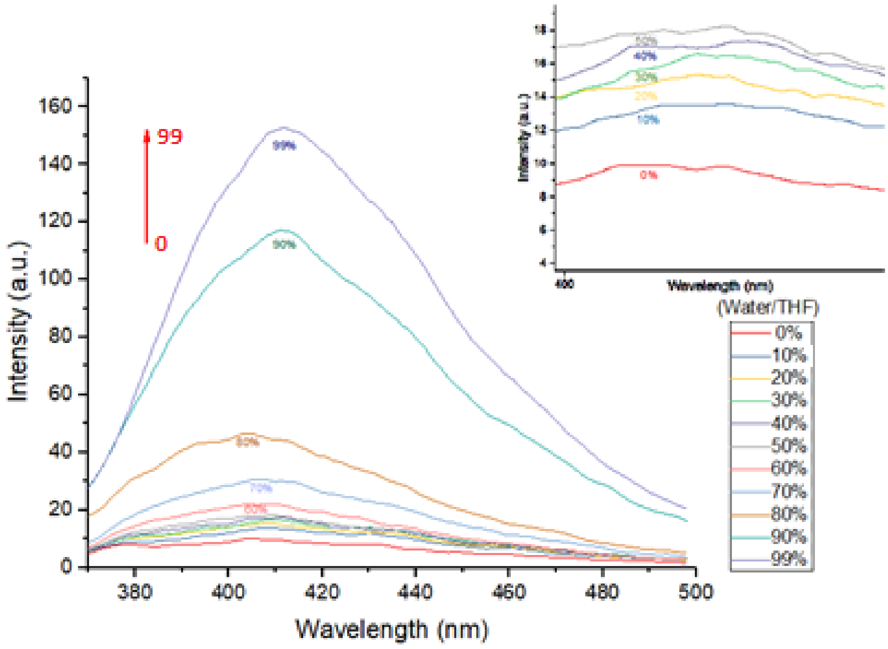

Figure B.1. Fluorescence spectrum of compound **3**.

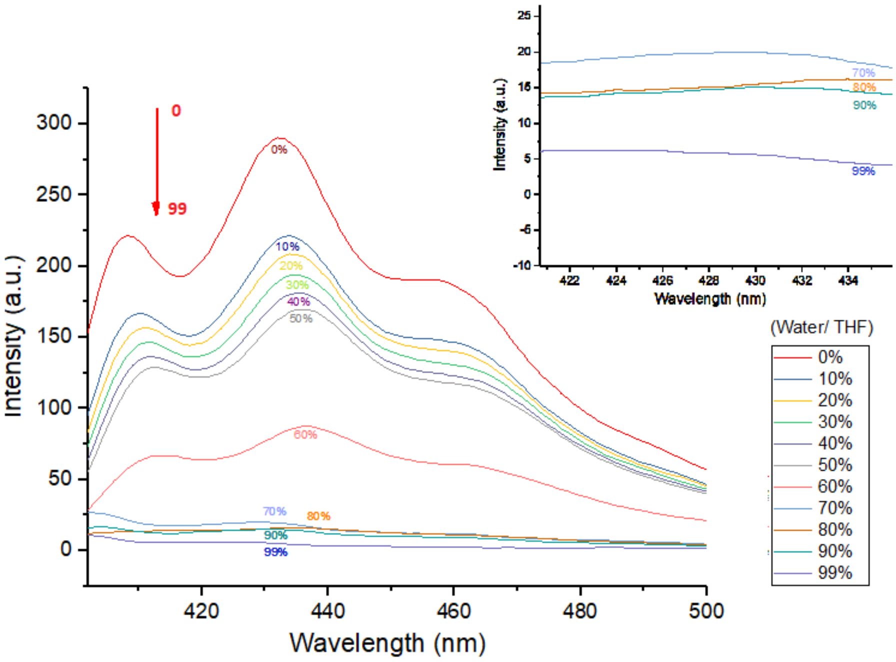

Figure B.2. Fluorescence spectrum of compound **11**.

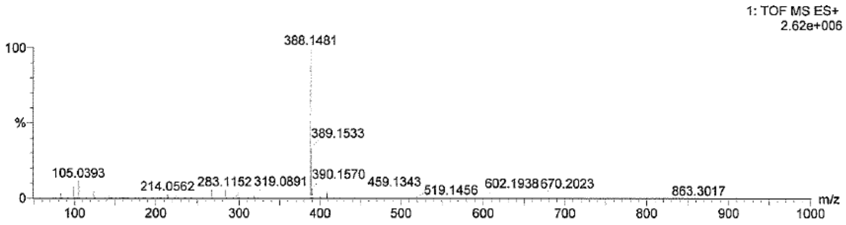

Figure B.3. HRMS chromatogram of compound **11.**

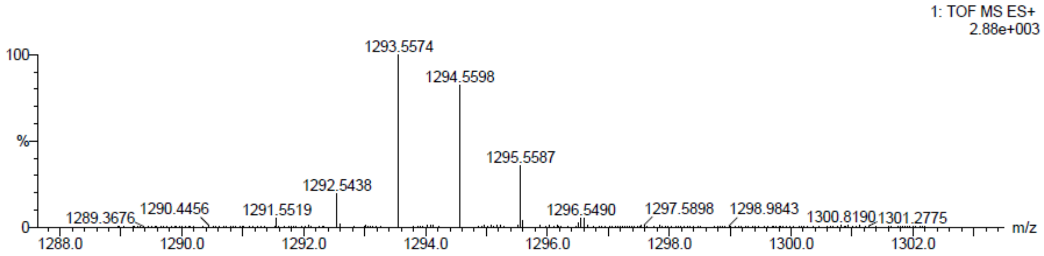

Figure B.4. HRMS chromatogram of compound **29**.

C. Appendix C

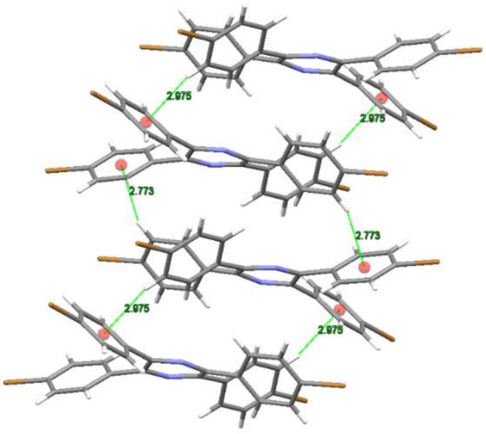

Figure C.1. Intermolecular C-H··π interactions between compound **27**.

Table C.1. *Experimental Details of Single crystal analysis of **27***.

Crystal data	
Chemical formula	$C_{28}H_{16}Br_4N_2$
M_r	700.03
Crystal system, space group	Monoclinic, $P2_1/c$
Temperature (K)	293
a, b, c (Å)	9.3412(2), 27.4868(8), 10.6524(7)
β (°)	105.475(7)
V (Å^3)	2636.0(2)
Z	4
Radiation type	Mo $K\alpha$
μ (mm^{-1})	6.13
Crystal size (mm)	0.95 × 0.75 × 0.22
Data collection	
Diffractometer	Rigaku RAXIS conversion
Absorption correction	–

No. of measured, independent and observed [$I > 2\sigma(I)$] reflections	65875, 6513, 3473
R_{int}	0.093
$(\sin \theta/\lambda)_{\text{max}}$ (Å^{-1})	0.666
Refinement	
$R[F^2 > 2\sigma(F^2)]$, $wR(F^2)$, S	0.064, 0.200, 1.12
No. of reflections	6513
No. of parameters	307
H-atom treatment	H-atom parameters constrained
$\Delta\rho_{\text{max}}$, $\Delta\rho_{\text{min}}$ (e Å^{-3})	0.80, −1.08

Table C.2. *Bond Lengths (Å) of compound* ***27***.

Br1—C8	1.881(5)	C9—C10	1.377(7)
Br2—C14	1.898(5)	C11—C12	1.388(6)
Br3—C20	1.898(5)	C11—C16	1.395(6)
Br4—C26	1.887(5)	C12—C13	1.367(6)
N1—C1	1.341(5)	C13—C14	1.367(7)
N1—C2	1.339(5)	C14—C15	1.374(7)
N2—C3	1.349(5)	C15—C16	1.387(7)
N2—C4	1.342(5)	C17—C18	1.395(6)
C1—C4	1.416(6)	C17—C22	1.388(6)
C1—C5	1.483(6)	C18—C19	1.383(7)
C2—C3	1.411(6)	C19—C20	1.368(8)
C2—C23	1.487(6)	C20—C21	1.379(7)
C3—C17	1.481(6)	C21—C22	1.380(7)
C4—C11	1.484(6)	C23—C24	1.389(6)
C5—C6	1.386(6)	C23—C28	1.392(6)
C5—C10	1.375(6)	C24—C25	1.395(6)
C6—C7	1.385(6)	C25—C26	1.384(7)
C7—C8	1.364 (7)	C26—C27	1.376(7)
C8—C9	1.381(7)	C27—C28	1.379(6)

Table C.3. *Bond Angles (˚) of compound* ***27****.*

C2—N1—C1	119.6(4)	C15—C14—Br2	119.5(4)
C4—N2—C3	119.0(4)	C14—C15—C16	119.4(5)
N1—C1—C4	119.5(4)	C15—C16—C11	120.5(4)
N1—C2—C3	120.2(4)	C22—C17—C18	118.3(4)
N2—C3—C2	119.8(4)	C19—C18—C17	120.4(5)
N2—C4—C1	120.4(4)	C20—C19—C18	120.1(5)
C10—C5—C6	117.5(4)	C19—C20—Br3	120.8(4)
C7—C6—C5	121.5(4)	C19—C20—C21	120.7(5)
C8—C7—C6	119.3(5)	C21—C20—Br3	118.5(4)
C7—C8—Br1	119.4(4)	C20—C21—C22	119.3(5)
C7—C8—C9	120.7(5)	C21—C22—C17	121.2(5)
C9—C8—Br1	119.8(4)	C24—C23—C28	118.7(4)
C10—C9—C8	119.0 (4)	C23—C24—C25	120.9(4)
C5—C10—C9	122.0(4)	C26—C25—C24	118.9(4)
C12—C11—C4	120.2(4)	C25—C26—Br4	119.3(4)
C12—C11—C16	118.1(4)	C27—C26—Br4	119.9(4)
C13—C12—C11	121.1(4)	C27—C26—C25	120.8(4)
C12—C13—C14	120.1(4)	C26—C27—C28	120.1(5)
C13—C14—Br2	119.8(4)	C27—C28—C23	120.6(4)
C13—C14—C15	120.7(4)		

Table C.4. *Selected Torsion Angles (˚) of compound* ***27****.*

C6—C7—C8—Br1	−176.0(4)	Br3—C20—C21—C22	−179.4(4)
Br2—C14—C15—C16	−179.4(4)	N1—C1—C4—C11	169.9(4)
C5—C1—C4—N2	169.0(4)	N1—C2—C23—C24	−41.9(6)
N2—C3—C17—C22	−41.0(6)	C24—C25—C26—Br4	−179.0(4)